Piezo1 mechanosensing regulates integrin-dependent chemotactic migration in human T cells

Chinky Shiu Chen Liu[1], Tithi Mandal[2], Parijat Biswas[3], Md. Asmaul Hoque[1,4], Purbita Bandopadhyay[1,4], Bishnu Prasad Sinha[1,4], Jafar Sarif[1,4], Ranit D'Rozario[1,4], Deepak Kumar Sinha[3], Bidisha Sinha[2], Dipyaman Ganguly[1]*

[1]IICB-Translational Research Unit of Excellence, CSIR-Indian Institute of Chemical Biology, Kolkata, India.

[2]Department of Biological Sciences, Indian Institute of Science Education and Research, Kolkata, India.

[3] Department of Biological Sciences, Indian Association for Cultivation of Science, Kolkata, India.

[4]Academy of Scientific and Innovative Research, Ghaziabad, India.

Correspondence: dipyaman@iicb.res.in

Running title: Piezo1 mechanosensing in human T cell chemotaxis

Keywords: Human T cells, Piezo1, Mechanosensing, Migration, Chemokine, Chemotaxis, Focal adhesion kinase, LFA-1, F-actin, Confocal Microscopy, Interference Reflection Microscopy

ABSTRACT

T cells are crucial for efficient antigen-specific immune responses and thus their migration within the body, to inflamed tissues from circulating blood or to secondary lymphoid organs, play a very critical role. T cell extravasation in inflamed tissues depends on chemotactic cues and interaction between endothelial adhesion molecules and cellular integrins. A migrating T cell is expected to sense diverse external and membrane-intrinsic mechano-physical cues, but molecular mechanisms of such mechanosensing in cell migration are not established. We explored if the professional mechanosensor Piezo1 play any role during integrin-dependent chemotaxis of human T cells. We found that deficiency of Piezo1 in human T cells interfered with integrin-dependent cellular motility on ICAM-1-coated surface. Piezo1 recruitment at the leading edge of moving T cells is dependent on and follows focal adhesion formation at the leading edge and local increase in membrane tension on chemokine receptor activation. Piezo1 recruitment and activation, followed by calcium influx and calpain activation, in turn are crucial for the integrin LFA-1 (CD11a/CD18) recruitment at the leading edge of the chemotactic human T cells. Thus, we find that Piezo1 activation in response to local mechanical cues constitutes a membrane-intrinsic component of the 'outside-in' signaling in human T cells, migrating in response to chemokines, that mediates integrin recruitment to the leading edge.

INTRODUCTION

Efficient T cell migration from blood circulation to secondary lymphoid organs and inflamed tissue is paramount for optimal tissue antigen sampling and effector functions during adaptive immune response (1-4). The process is dependent on chemotactic cues, interaction between endothelial adhesion molecules and T cell integrins, and an intricate acto-myosin dynamics (5). Generation of mechanical force is critical to propel migrating cells (6-9). Mechanosensing of the substrate and increase in cellular membrane tension is also intuitively apparent in a migrating T cell, although mechanistic details are not explored to a great extent.

Piezo1 and Piezo2 ion channels are evolutionarily conserved professional mechanosensors that can sense increase in membrane tension mostly independent of other protein-protein interactions (10-12). Mechanosensing by Piezo1 has been demonstrated to play critical role in diverse patho-physiologic contexts given its wide tissue expression including the immunocellular compartment (13-21). We previously identified crucial role of this specialized mechanotransducer in optimal TCR triggering (14, 19). The immunocellular expression of Piezo1 thus makes it a strong candidate for mechanosensing at the plasma membrane to regulate motility of immune cells. Piezo1 shows differential involvement in cellular migration depending on context (22- 28). Previous studies point to the possibility of a role of Piezo1 in confinement sensing and integrin activation in moving cells, while it deters integrin-independent cell motility, usually referred to as amoeboid movement (29, 30).

Here we aimed at exploring if Piezo1 mechanosensing plays any role during integrin-dependent chemotactic migration of human T cell migration, a patho-physiologically critical event in an ongoing immune response as well as in the steady-state. We found that deficiency of Piezo1 expression in human $CD4^+$ T cells as well as Jurkat T cells interfered with efficient integrin-dependent cellular motility in response to a chemotactic cue. We also found that Piezo1 activation constitutes a hitherto unknown membrane-intrinsic component of the 'outside-in' signaling in human T cells in response to chemokine receptor activation, that follows activation of focal adhesion kinase leading to local increase in membrane tension and mediates local recruitment of integrin molecules at the leading edge of the moving human T cells.

RESULTS

Piezo1 deficiency abrogates integrin-dependent chemotactic motility in human T cells

65 We first assessed the role of Piezo1 on integrin-dependent, non-directional motility of primary human
66 $CD4^+$ T cells. We used GFP plasmid and Piezo1 siRNA co-transfected cells to facilitate distinction
67 between potentially transfected and untransfected cells during cell tracking. We compared the
68 motility of GFP^+ T cells (presuming they had a good transfection efficiency and thus will also have the
69 siRNA) with the GFP^- T cells in the same culture. This was confirmed by flow cytometric assessment of
70 Piezo1 protein content on the T cell surface as well as the whole T cells (Supplemental figures 1B, C).
71 Piezo1 deficiency in T cells (potentially GFP^+) significantly hindered their migration in response to
72 CCL19 in terms of its mean-squared displacement (MSD, Figure 1A-C). Representative cell tracks of
73 Piezo1 deficient (GFP^+) and control (GFP^-) are shown in Figure 1B, supplementary figure 1D and
74 supplemental video 1. These results were further confirmed in a separate experiment where Piezo1
75 KD cells showed significant reduction in motility compared to control siRNA-transfected cells
76 (Supplementary figure 1E).

77 ICAM1-coated transwell chemotaxis assay of human $CD4^+$ T lymphocytes and Jurkat T cells also
78 showed significant reduction in migration upon siRNA-mediated Piezo1 knockdown, in response to
79 CCL19 and SDF1α gradients, respectively (Figure. 1D, E). Piezo1 inhibition with GsMTx4 also led to
80 significant impairment of transwell chemotaxis (Supplementary figure 1F).

81

82 **Redistribution of Piezo1 toward the leading edge of migrating T cells in response to chemotactic cue**

83 Cell polarity is a crucial aspect of directional cell motility in response to chemokines. $CD4^+$ T cells
84 seeded on ICAM-1 bed showed striking polarity in Piezo1 distribution, upon stimulation with CCL19
85 for 15 minutes (Figure 1F, G; Supplemental video 2). Piezo1 m-Cherry expressing Jurkat T cells also
86 showed striking leading edge polarity in the presence of SDF1α under ICAM1 adhesion (Figure 1H). In
87 Figure 1I, particle image velocimetry (PIV) analysis of a single representative Jurkat cell has been
88 shown to display the dynamically polarized Piezo1 fluorescence upon SDF1α treatment with time, as
89 opposed to rather uniformly distributed Piezo1 signals in a representative untreated cell. The
90 continuous redistribution of Piezo1 within the motile T cells towards the leading edge can also be
91 appreciated in the representative moving image provided (Supplemental video 3).

92

93 **Piezo1 redistribution in migrating T cells follow increased membrane tension in the leading edge**

94 Piezo1 is a professional mechanosensor ion channel, which senses increase in plasma membrane
95 tension and responds by driving calcium influx into the cells (14, 19, 31). As T cells migrate on substrate

96 by extending membrane processes, it is intuitive to hypothesize that a component of mechanosensing
97 is incorporated in the mechanism of cellular movement. The data above, on a critical role of Piezo1 in
98 migrating human T cells, also led us to hypothesize that Piezo1 mechanosensors may play a role in
99 sensing mechanical cues in a moving T cell. So, first we aimed at confirming that there is polarized
100 increase in tension in the leading edge plasma membrane of human T cells, moving in response to a
101 chemotactic cue.

102 Cellular membrane tension can be measured by various techniques. However, most of the usual
103 techniques, viz. atomic force microscopy or tension measurement using optical tweezers, are invasive
104 and interfere with the membrane dynamics, as well as are difficult to employ on moving cells. We
105 utilized the non-invasive technique of interference reflection microscopy or IRM for studying potential
106 redistribution of membrane tension following chemokine stimulation (32, 33). In IRM technique,
107 steady-state local fluctuations in the plasma membrane is imaged in cells adhered to a glass coverslip.
108 The interference patterns generated due to continuously changing local distance between the
109 coverslip and the plasma membrane are computed to derive the magnitude of local tension in the
110 membrane – lower temporal fluctuations represent an increase in membrane tension (Figure. 2A).
111 After baseline imaging, Piezo1-GFP expressing Jurkat cells were subjected to sequential fluorescence
112 and IRM imaging post SDF1α addition which was followed over time. Chemokine administration to
113 Jurkat T cells led to a decrease in temporal fluctuations and an increase in membrane tension when
114 computed for the whole cellular contour (Figure 2B). The increase in membrane tension was
115 registered within few minutes after chemokine addition and gradually declined over time (Figure 2C).
116 Distribution of tension and fluctuation-amplitude in cells was also affected by the action of chemokine
117 (Supplemental figure 2A) which was accompanied by increase in the membrane's degree of
118 confinement and the effective viscosity experienced (Supplemental figure 2C & D). Moreover, the
119 tension maps showed that the lamellipodial structures towards the leading edges of the cells had
120 higher tension magnitudes (Figure 2D, Supplemental figure 2B). These high-tension edges are usually
121 further emphasized at later time-points.

122 Finally, we explored if local membrane tension increase was linked to Piezo1 redistribution in the
123 chemokine-experienced T cells. Of note here, during acquisition, there is typically a time delay of 1
124 minute between measurement of tension and Piezo1-GFP fluorescence. As expected, average tension
125 peaked within the first few minutes of chemokine addition, followed by partial decline (Figure 2E) as
126 seen for the whole cell. Pixel count of Piezo1-GFP intensity showed a similar pattern, albeit, at a
127 delayed time, following the tension kinetics. In order to account for the delayed kinetics of tension
128 magnitude and Piezo1-GFP pixel count, we performed a correlation between normalised Piezo1 pixel

129 intensity at a particular time-frame, with normalised tension magnitude at the preceding time frame.
130 We observed significant positive correlation between the two parameters (Figure 2F, G). Thus, IRM-
131 coupled fluorescence microscopy revealed an increase in local membrane tension in the leading edge
132 of the moving T cells in response to chemokine receptor activation that was associated with Piezo1
133 redistribution to the leading edges of the cells.

134

135 **Focal adhesion following chemokine receptor activation does not depend on Piezo1**

136 Focal adhesion formation is a critical step in cellular migration and activated phosphorylated focal
137 adhesion kinases link extracellular physical cues to the cytoskeletal actomyosin scaffold (34, 35).
138 Chemokine signaling induces phosphorylation of focal adhesion kinase (FAK) and membrane
139 recruitment of the FAK complex forming focal adhesions with the extracellular substrate. FAK recruits
140 adapter proteins like paxillin to anchor with the local sub-membrane cytoskeleton made by de novo
141 F-actin polymerization. Membrane-recruited FAK complexes anchored to cytoskeleton increases local
142 membrane tension as well as recruit integrins to the membrane (36, 6, 37). This so-called 'outside-in'
143 signaling, whereby membrane recruitment of integrins (e.g.; LFA1 in T cells) is initiated, is followed by
144 integrin signaling ('inside-out' signaling) driven primarily by phosphoinositide 3-kinase (PI3K)-driven
145 phosphorylation of Akt and downstream activation of Rho GTPases which in turn drive extensive F-
146 actin polymerization (38, 39). Retrograde flow of the F-actin to the rear end of the moving cells,
147 through myosin-based contractions, generates the propelling force for cells to move forward following
148 the chemokine gradient (6, 7).

149 Finding a critical role of Piezo1 in human T cell migration and a membrane tension-dependent
150 redistribution of Piezo1 to the leading edge of the moving cells led us explore if FAK recruitment to
151 the leading edge in response to chemokine stimulation was dependent on Piezo1. While
152 phosphorylated FAK (pFAK) showed striking polarity upon CCL19 stimulation on ICAM-1 beds (Figure
153 3A, B, Supplementary video 4), Piezo1 knockdown did not have any effect on pFAK polarity under the
154 same conditions (Figure 3C, D). We observed similar results upon examining distribution of paxillin
155 which is another critical component of focal adhesions. Paxillin showed increased polarity upon CCL19
156 stimulation (Figure 3E, F) and its polarity remained unaffected upon Piezo1 KD (Figure 3G, H). We also
157 did not observe any changes in pFAK and paxillin signal intensity upon Piezo1 knockdown in CCL19-
158 stimulated cells (Supplementary figure 3A, B, respectively). However, pFAK showed striking co-
159 localization with Piezo1 upon CCL19 stimulation (Supplementary figure 3C). Thus, focal adhesion
160 formation following chemokine receptor activation was not dependent on Piezo1. FAK activation

161 recruits adapters like paxillin and vinculin connecting the cortical cytoskeleton to the membrane and
162 the extracellular matrix, thereby increasing local membrane tension (34). Inhibition of FAK activation
163 completely abrogated Piezo1 redistribution to the leading edge, hence the polarity (Figure 3I, J). This
164 indicated that mechanistically, FAK activation event precedes Piezo1 redistribution to the leading edge
165 of the migrating human $CD4^+$ T cells.

166

167 **Membrane recruitment of LFA1 on chemokine receptor activation disrupts with Piezo1 deficiency**

168 Integrin recruitment to the leading edge occurs downstream of FAK activation and local F-actin
169 polymerization. As expected, CCL19 stimulation led to LFA1 recruitment to the leading edge upon
170 CCL19 stimulation on ICAM1 bed (Figure 4A, B; Supplemental video 5). Moreover, Piezo1 and LFA1
171 (CD11a) exhibited significant colocalization upon chemokine stimulation (Figure 4C). Piezo1
172 downregulation abrogated LFA-1 polarity (Figure 4D, E; Supplemental videos 6, 7). Thus, role of Piezo1
173 in chemotactic migration of T cells was downstream of FAK assembly in response to chemokine
174 receptor signaling, but preceded integrins recruitment. These data together point to a mechanism
175 whereby local increase in membrane tension leading from FAK activation and assembly drives Piezo1
176 activation, which in turn is linked to LFA1 recruitment to the focal adhesions.

177 To further confirm this critical role of Piezo1 on LFA1 recruitment, we looked at the major signaling
178 event downstream of LFA1 recruitment to the leading edge, i.e., phosphorylation of Akt downstream
179 of PI3K activation, which in turn is triggered upon integrin activation. On treatment with CCL19, human
180 $CD4^+$ T cells moving on ICAM-1-coated plates did show a prominent leading-edge polarity of non-
181 phosphorylated and phosphorylated Akt (pAkt) (Figure 4F, control panel). But in Piezo1-deficient cells
182 the polarity of pAkt is abrogated (Figure 4G), not affecting the polarity of non-phosphorylated AKT
183 (Figure 4H; Supplemental videos 8, 9), substantiating the cellular signaling defect due to non-
184 recruitment of LFA1 to the leading edge membrane.

185 **Piezo1 deficiency disrupts F-actin retrograde flow in T cells despite chemokine receptor activation**

186 Piezo1-mediated sensing of membrane tension drives calcium ion influx, which in turn has been shown
187 to activate calpain and F-actin polymerization (14, 19). LFA1 recruitment is driven by local actin
188 scaffold formation following FAK assembly, which as our data indicates is perhaps contributed by
189 consolidation local actin scaffold downstream of Piezo1 activation. To confirm this, we performed Ca^{2+}
190 imaging in Piezo1-mCherry transfected Jurkat Cells using total internal reflection fluorescence (TIRF)
191 microscope in response to chemokine. We found significant colocalization of the Ca^{2+} signal with the
192 Piezo1 signal on the chemokine treated Jurkat cells (Figure 5A, B; Supplemental figure 4A, B). Next to

193 confirm that activation of calpain mediates the Piezo1 function, we observed that prior inhibition with
194 calpain inhibitor PD150606 abrogated CCL19-induced LFA1 recruitment to the leading edge of the T
195 cells (Figure 5C, D). As expected, the upstream event of pFAK polarity was not affected by the calpain
196 inhibition (Supplemental figure 4C, D).

197 While F-actin polymerization downstream of FAK is required for LFA1 recruitment, LFA1 in turn drives
198 a more robust F-actin polymerization at the leading edge, through Akt/Rho GTPase activation. Leading
199 edge F-actin undergoes retrograde flow due to myosin contractions, thereby enabling cells to move
200 forward. Thus, both at the leading edge lamellipodia and the rear edge F-actin redistribution can be
201 documented in a motile cell. We observed focal co-localization of LFA1 with F-actin at the leading
202 edge, along with a denser actin-rich protrusion in the rear edge or the uropod (Figure 5C), which was
203 abolished upon calpain inhibition (Figure 5C, E). Hence, LFA1 recruitment may depend on local F-actin
204 polarization downstream of Piezo1 activation. On the other hand, failure of LFA1 recruitment and
205 activation halts further F-actin polarization feeding the retrograde flow of actin during migration.

206 Dichotomy of Piezo1 (dense leading edge distribution) and F-actin (more dense at the rear end)
207 distribution was clearly demonstrated in cells stimulated with chemokine (Figure 6A and Supplemental
208 video 10). But, no F-actin polarity was seen on downregulating Piezo1 in the T cells (Figure 6B, C;
209 Supplemental videos 11, 12). Live cell imaging of Jurkat T cells expressing Piezo1-mCherry and actin-
210 GFP on ICAM-1 coated dishes was performed in the presence or absence of SDF1α (Supplemental
211 figure 5A). Chemokine addition showed significant increase in Piezo1 polarity to the front end, as
212 shown in the earlier experiments (Figure 6E, Supplemental figure 5B, left) upon chemokine stimulation
213 when compared to untreated cells (Figure 6D, Supplemental figure 5B, left). But F-actin showed a
214 dynamic balance at both ends as expected (Figure 6E, Supplemental figure 5B, right). Polar plots
215 depicting angular distribution of Piezo1 mCherry and actin-GFP (over all time-points) in the presence
216 or absence of SDF1α are shown in Supplemental figure 5C. Representative image 6F and supplemental
217 video 13 shows Piezo1-mCherry distribution predominantly at the leading edge and actin-GFP
218 eventually accumulating at the rear end in uropod-like cellular extensions in a migrating Jurkat T cell.

219 Thus, our data reveals a membrane-intrinsic event, involving a critical role of Piezo1 mechanosensors,
220 within the outside-in signaling module in response to chemokine receptor activation in human T cells.
221 The mechanistic model derived from our data is depicted in Figure 7. The Piezo1 mechanosensing links
222 the focal adhesion assembly to integrins recruitment at the leading edge of the human T cells
223 migrating in response to chemokine activation and thus play a critical role in chemotactic migration of
224 human T cells.

225

226 **DISCUSSION**

227 The present study explored the role of membrane-intrinsic tension generation and the crucial role of
228 sensing this physical cue in the context of human T cell migration in response to chemokine receptor
229 activation. Deficiency of Piezo1 inhibited integrin-dependent migration, demonstrating crucial role of
230 these mechanosensors in this mode of T cell migration. As the integrin-dependent chemotactic
231 migration of T cells is a critically implicated in most patho-physiologic contexts, in the present study
232 we focused on the potential role of Piezo1 mechanosensors in this specific context.

233 Notably, a previous study in vivo in mice, using genetic deletion of Piezo1 in T cells, reported no
234 significant effect on tissue recruitment of T cells (17). Although a functional redundancy in the role of
235 Piezo1-mediated mechanosensing in mouse T cells warrants exclusion, especially in case of gene
236 deletion in developing T cells, given the considerable expression of Piezo2 as well in mouse T cells (40).
237 On the other hand, a role of Piezo1 activation in fibroblastic reticular cells in Peyer's patches has been
238 shown to regulate lymphocyte migration through tissue conduits (41). The different tissue distribution
239 of Piezo1 and Piezo2 expression in humans warranted exploring the role of Piezo1 in migrating human
240 T cells, as in humans Piezo2 is hardly expressed in the hematopoietic cells.

241 Non-invasive interference reflection microscopy allowed us to demonstrate dynamic change in
242 membrane tension at the leading edge of T cells stimulated with chemokine on ICAM1-bed which was
243 closely followed by dynamic recruitment Piezo1 locally. Chemokine receptor activation leads to focal
244 adhesion formation at the leading edge of the migrating T cells (34, 35). Our experiments revealed
245 that Piezo1 recruitment at the leading edge of the cells followed focal adhesion kinase activation.
246 Focal adhesions do increase local membrane tension as they connect the extracellular environment
247 with the cortical cytoskeleton of the cell (34). Piezo1 recruitment locally seems to be a response to
248 this membrane tension increase at focal adhesions. Piezo1 recruitment to focal adhesions was also
249 shown to play a role in enhancing glioblastoma aggression by activating integrin-FAK signalling
250 upstream of ECM remodelling and tissue stiffening (42). Interestingly, recent study by Yao et. al.,
251 showed that Piezo1 is required for formation of mature focal adhesions. Piezo1 binds to matrix
252 adhesion regions in a force-dependent manner via a linker domain and this binding is abrogated in
253 cancer cells causing transformation to malignant phenotypes (43).

254 'Outside-in' signaling downstream of focal adhesion formation recruits integrins to the leading edge
255 of the moving T cells (35, 36) which was abrogated by Piezo1 downregulation. Piezo1 has been shown
256 to drive Ca^{2+} influx into the T cells leading to calpain activation (14, 19). As expected, calpain inhibition

257 also interfered with leading edge recruitment of the integrin LFA-1. Plausibly calpain activation drives
258 local F-actin polymerization at the leading edge facilitating LFA-1 recruitment. This was also supported
259 by loss of polarity of AKT phosphorylation with Piezo1 deficiency, which is known to be the major
260 downstream signaling module that succeeds LFA-1 recruitment and activation (39, 44). These
261 dysregulations in turn abrogates the retrograde flow of actin in the moving cell that is essential for
262 forward propulsion of the cell body (6, 7, 37, 43). Of note here, a role of ER-resident Piezo1, in driving
263 R-RAS-driven activation of integrins, which was again dependent on calpain activation, was reported
264 even before the mechanosensing function of Piezo1 was established (30).

265 Thus, the present study reports a hitherto unexplored role of the professional mechanosensor Piezo1
266 in integrin dependent chemotactic movement of human T cells. In the cascade of leading edge events
267 in a moving human T cell, following chemokine receptor activation and eventually leading to the
268 retrograde flow of actin, focal adhesion formation precedes Piezo1 activation, while LFA-1 recruitment
269 is dependent on Piezo1 function.

270

271 **METHODS**

272 **Human CD4$^+$ T cell isolation and transfection.**

273 Human CD4$^+$ T lymphocytes were isolated from peripheral blood from healthy donors through
274 magnetic immunoselection. Peripheral blood samples from healthy human subjects were collected on
275 obtaining written informed consents. The studies were approved by the Human Ethics Committee of
276 CSIR-Indian Institute of Chemical Biology, India. Cells were transfected with either EGFP control or
277 Piezo1-specific siRNAs using Lonza 4D nucleofector, as per the manufacturer's protocol. Briefly, cells
278 were nucleofected in 100µl of supplemented P3 primary buffer containing 175ng of respective siRNAs.
279 Nucleofection was performed using EO-115 pulse in Lonza 4D nucleofector. Nucleofected cells were
280 incubated at 37°C. 5% CO_2 in RPMI media containing 10% FBS for 3 days before experiments were
281 conducted. Knockdown was checked by qPCR measurement of Piezo1 and Piezo2 transcript levels
282 (Supplementary Figure. 1A).

283 GFP/Piezo1 siRNA co-nucleofection

284 Approximately 2×10^6 human CD4+ T lymphocytes were nucleofected with 3µg of GFP-expressing
285 plasmid along with 175ng of Piezo1-specific siRNA. Cells were incubated for 3 days before migration
286 studies. EGFP esiRNA was used as control siRNA in experiments involving comparison between control
287 and Piezo1 siRNA-KD cells.

288 Analysis of Piezo1 knockdown

289 GFP and Piezo1 siRNA co-transfected $CD4^+$ T cells were stained for Piezo1 to measure downregulation.
290 Both surface and intracellular (0.2% triton X-100 permeabilization) Piezo1 were stained. Briefly, cells
291 were collected on day and fixed in 0.5% PFA for 5 minutes on ice. Cells were stained with 1.67µg/ml
292 of rabbit anti-Piezo1 for 45 minutes at 4°C. After washing, 1.5µg/ml of anti-rabbit alexa 568-IgG was
293 added and incubated for 30 minutes at 4°C. Cells were acquired on BD LSR Fortessa III after washing.
294 Piezo1 mean fluorescence intensity (MFI) were measured both for GFP^+ and GFP^- cells.

295 **2-dimensional cell tracking.**

296 12-mm confocal dishes were coated with 4µg/ml of recombinant human ICAM-1 overnight at 4°C.
297 Wells were washed with 1X PBS. Tracking of GFP/Piezo1 siRNA-transfected cells were performed after
298 cell trace violet-labelling in the presence of recombinant CCL19 on ICAM1-coated dishes. Stained cells
299 were added to the wells and allowed to settle for 1 hour at 37°C. 2D tracking was performed at 37°C
300 after addition of 0.5µg/ml of recombinant human CCL19 and incubated for 10 minutes before
301 acquisition. Images were acquired at regular intervals at room temperature using Zeiss LSM setup at
302 20X magnification for a total duration of 10-15 minutes at 30 second interval. $CD4^+$ T lymphocytes
303 were RPMI without phenol red supplemented with 10% FBS and 25mM HEPES during the duration of
304 imaging.

305 **2D cell tracking analysis**

306 For tracking analyses of GFP and Piezo1 siRNA co-transfected cells, all cells above a specific threshold
307 area were used to eliminate potential debris and dead cells due to GFP plasmid transfection. Time-
308 based image stacks obtained were analysed using the Particle Tracker 2D/3D plugin of the FIJI Mosaic
309 Suite. Briefly, images were corrected for any shift in alignment during acquisition, using the StackReg
310 plugin. Corrected images were the thresholded to create a 0-255 binary mask which were then used
311 for tracking using the Particle Tracker 2D/3D plugin. Tracking provided frame-wise X-Y co-ordinates
312 of cells which were subsequently used to derive the following parameter to measure motility:

313 *a. Mean-squared displacement*

314 *MSD (n)* = $\sum_{i=0}^{i=n}(x_n - x_0)^2 + (y_n - y_0)^2$ where,

315 i = 0 is the first frame,

316 i = n is the nth frame.

317 **Tranwell chemotaxis assay**

318 5µm transwell inserts were coated with 4µg/ml of recombinant human ICAM-1. Equal number of
319 primary human $CD4^+$ T cells and Jurkat cells nucleofected with control or Piezo1-specific siRNA were
320 added to the ICAM-1-coated inserts. Cells were allowed to migrate in response to recombinant human
321 CCL19 (0.5µg/ml) or SDF1α (0.1µg/ml) in the lower chamber wells for 5 hours and 1.5 hours,
322 respectively, at 37°C, 5% CO_2. Migration was halted by placing the setup on ice. Percent migration was
323 calculated by counting the number of cells in the lower chamber and dividing it by total number of
324 cells that was seeded.

325 **Overexpression of mCherry/GFP-tagged Piezo1 and Actin-GFP in Jurkat cells.**

326 GFP and mCherry-tagged Piezo1 constructs were kindly provided by Dr. Charles Cox at Victor Chang
327 Cardiac Research Laboratory, Darlinghurst, Australia. Approximately 2 million Jurkat cells were
328 nucleofected with 2-3µg of fluorescent Piezo1 construct in 100µl of supplemented SE cell line buffer.
329 Cells were pulsed using CL-120 program in Lonza 4D nucleofector. Cells were cultured in antibiotics-
330 deficient RPMI supplemented with 20% FBS for 36 hours. Overexpression was confirmed using flow
331 cytometry.

332 **Interference Reflection Microscopy and Analysis**

333 Jurkat cells were nucleofected with 2-3µg/ml of Piezo1-GFP construct. Overexpression was confirmed
334 using flow cytometry. Transfected cells were seeded on recombinant human fibronectin glass-based
335 dishes. Cells were allowed to completely adhere for 1 hour to allow IRM imaging.

336 An inverted microscope (Nikon, Japan) with 60x 1.2 NA water-immersion objective, Hg arc lamp and
337 necessary interference filter (546 ± 12 nm) were used for the interference reflection microscopy (45,
338 46) and images were captured at 19.91 frames per second using a EMCCD camera (Evolve 512 Delta;
339 Photometrics, Trenton, NJ). Cells that were significantly adhered to the glass bottom were used for
340 imaging. Regions used for analysis were stringently chosen to avoid parts farther than ~ 100 nm from
341 the coverslip – also called the first branch region (FBR) and the size chosen was 4x4 pixels
342 corresponding to ~ $(720\ nm)^2$. First, cells were imaged by IRM to take baseline reading following which
343 chemokine (SDF1α) was added. Cells were followed till 30 min with ~ 2-3 min interval post-chemokine
344 addition.

345 For stringent selection of subset of regions, extraction of parameters as well as for visualizing the
346 amplitude of fluctuations, the methodology developed previously (46, 47) was followed. 2048 frames
347 corresponding to ~ 102 sec were captured and used for a single measurement of tension. The analysis

348 involved calculation of standard deviation of temporal height fluctuations (SD_{time}) and estimating the
349 power spectral density (PSD) by autoregressive technique (probability of covariance or pcov) where
350 the order is chosen to match best with PSD obtained using fast fourier transform (MATLAB, Mathworks
351 Inc., USA). For deriving mechanical parameters, the PSD is fitted with a Helfrich-based model –

352
$$PSD(f) = \frac{4\eta_{eff} A k_B T}{\pi} \int_{q_{min}}^{q_{max}} \frac{dq}{(4\eta_{eff}(2\pi f))^2 + \left[\kappa q^3 + \sigma q + \frac{\gamma}{q}\right]^2}$$

353 with four fitting parameters (46) using fluctuation-tension (σ), effective viscosity (η_{eff}), level of
354 confinement (γ) and the effective active temperature (A)). The bending rigidity (κ) was fixed at 15 k_BT.
355 Membrane fluctuation-tension closely follows membrane frame tension for a large range of tension
356 values (48). Membrane fluctuation-tension closely follows membrane frame tension for a large range
357 of tension values (48). For brevity, membrane fluctuation-tension has been referred to as "tension" in
358 the rest of the manuscript. Tension maps were created from PSDs calculated for every pixel which
359 were subsequently fitted and parameters extracted for every pixel. For analysing correlation between
360 fluorescence and tension, first the fluorescence distribution of cells was plotted. Regions of
361 intermediate intensity (around the first peak of the distribution) of a fixed intensity range was filtered
362 and the pixel count of the filtered area was plotted against the average tension in those pixels.
363 Normalization was done by diving by the maximum value in the time series. Normalized pixel count,
364 thus, reflects how area with high Piezo1-GFP at the membrane changes while avoiding a small area
365 fraction with very high Piezo1-GFP which might arise from internal structures. To ensure significance
366 of the observed differences, the statistical test undertaken was the Mann-Whitney U test.

367 **Piezo1 and actin distribution in live cell imaging**

368 Jurkat cells expressing mCherry-tagged Piezo1 were seeded on ICAM-1-coated dishes. 0.1µg/ml of
369 recombinant human SDF1α was added to the cells for 15 minutes prior to imaging. Cell tracking was
370 performed in EVOS FL microscope using the PE-Texas red filter, at an interval of 1 frame per minute,
371 at room temperature. Imaging was performed for a total duration of 15 minutes.

372 For Jurkat cells transfected with Piezo1-mcherry and actin-GFP, cells were treated similarly and
373 acquired on Zeiss LSM confocal setup. Z-stack was obtained at 1µm per stack to capture the entire
374 cell. Time-lapse was imaged at an interval of 30 second per frame for a total duration of 5 minutes.
375 Confocal imaging was performed at 37°C.

376 For particle image velocimetry (PIV) analysis of Piezo1-mCherry-expressing Jurkat cells was performed
377 using the Iterative PIV plugin of FIJI. Time-lapse image stacks were split and stacks of paired

378 subsequent images were formed. Each of these stacks was then corrected for any shift in alignment
379 using the StackReg plugin. Aligned stacks were then subjected to iterative FIJI PIV analysis using the
380 conventional cross-correlation method to measure flow of fluorescent Piezo1 in chemokine-treated
381 Jurkat cells. PIV post-processing was done with default parameters and PIV magnitude plots were
382 obtained from the plugin.

383 **Measurement of cell polarity during live-cell imaging.**

384 A custom code was written in Fiji (ImageJ) to analyze the cell image time-lapse for the calculation
385 Front/Back (F/B) ratio of actin and Piezo1 expression relative to the direction of cell migration. Briefly,
386 intensity-based thresholding was performed on the actin images to create binary masks of the cells.
387 Individual cell boundaries were identified in the time-lapse, which were stored in the form of polygon
388 ROIs. The cell ROIs enabled the computation of each cell's trajectory and displacement vectors from
389 the geometrical centroid at every frame of the time-lapse video. The computation of cell polarity
390 involved fitting each cell's ROI to an ellipse and bisecting the ellipse perpendicular to the migration
391 direction. The ratio of total intensities in the leading half and the trailing half of the ellipse was
392 calculated for actin and piezo1 images to get the F/B ratio.

393 For polarity measurement of fixed confocal images, cell boundaries were similarly identified. Stored
394 ROIs were then split into two halves perpendicular to the long axis of the cell. The polarity index was
395 measured by calculating the difference of total intensities of two halves of the cell divided by the sum
396 of their total intensities. A measurement of 1 shows complete skewing of fluorescent signals to one
397 half of the cell, while a value of 0 shows uniform distribution of fluorescent signals in both cell halves
398 Representative polarity analysis Piezo1 (fixed), Piezo1 mCherry (live), pFAK (fixed), CD11a/LFA-1
399 (fixed) and actin (fixed) of untreated and CCL19-stimulated $CD4^+$ T lymphocytes (Supplemental figure
400 6A-F).

401 **Generation of Piezo1 mCherry and Actin-GFP polar plots.**

402 For analysis of angular/spatial distribution of Piezo1 mCherry and actin-GFP with respect to direction
403 of cell movement, cell ROIs were applied to the actin and piezo1 channels individually, to find the
404 intensity-weighted centre of mass (through all the time-points). Depending on the fluorescence
405 intensity distribution, the intensity-weighted centre of mass is shifted away from the geometric
406 centroid and towards the direction of a higher protein distribution. Thus, a vector connecting the
407 centroid (geometric centre) to the centre of mass gives the direction of polarization of the protein of
408 interest. The relative angle of the polarization vector against the cell displacement vector was

409 calculated for each frame, and a polar histogram of the angles was plotted for actin-GFP and piezo1-
410 mCherry.

411 **Fixed immunostaining for confocal imaging**

412 Untransfected human $CD4^+$ T lymphocytes were seeded on 12-mm, ICAM-1-coated glass coverslips at
413 a density of about 0.2 million cells per coverslip. Cells were incubated at 37°C, 5% CO_2 for 1.5 hours.
414 0.5µg/ml of recombinant human CCL19 was added to each coverslip and incubated for 20-30 minutes
415 at 37°C. Post-treatment, cells were fixed in 4% paraformaldehyde for 15 minutes at room
416 temperature. Blocking was performed in 3% bovine serum albumin in 1X PBS containing 0.2% Triton
417 X-100 for 50 minutes at room temperature. Primary rabbit anti-human Piezo1 (Proteintech) was
418 added at a dilution of 1:100 (5µg/ml) and incubated at room temperature for 1 to 1.5 hours. Alexa
419 568-conjugated anti-rabbit IgG was added at a dilution of 1:350 (5.7µg/ml), and incubated for further
420 45-50 minutes. Nuclear staining was performed for 1 minute with Hoechst 33342 dye at a
421 concentration of 1µg/ml in 1X PBS. All washes between steps were carried out in 1X PBS. Stained cells
422 were then mounted on Vectashield® mounting media and sealed before confocal imaging. For Piezo1
423 and CD44 co-staining, rabbit anti-Piezo1 and mouse anti-human CD44 were used at a concentration
424 of 5µg/ml, each. Alexa 488-conjugated anti-rabbit IgG and alexa 633-conjugated anti-mouse IgG were
425 used at a concentration of 5.7µg/ml, each.

426 For actin imaging, LifeAct-TagGFP2 protein was added at a concentration of 0.5µg/ml, and incubated
427 for 45 minutes at room temperature before washing. For LFA-1 ($\alpha_L\beta2$) staining, mouse anti-human
428 CD11a (α_L subunit) was added at a concentration of 5µg/ml, followed by addition of anti-mouse Alexa
429 594-conjugated IgG. For LFA-1 and Piezo1 co-staining, primary antibodies were added at above
430 concentrations, with Alexa 568-conjugated anti-rabbit IgG (for Piezo1) and Alexa 488-conjuagted anti-
431 mouse IgG (for CD11a/LFA-1). Rabbit/mouse anti-phosphorylated FAK (Tyr-397) and mouse Paxillin
432 was used to stain pFAK and paxillin, respectively to detect focal adhesions. These cells were treated
433 with chemokine CCL19 for 10 minutes prior to fixation. While doing confocal microscopy, Z-stacks
434 were captured at 0.5µm intervals. Confocal images are represented are maximum intensity
435 projections of the Z-slices. 3Dprojectionfunction of Fiji was used to create a 3D rendering of the Z-
436 slices, using the brightest point method of projection.

437 **TIRF Imaging and Ca^{2+}-Piezo1 colocalization**

438 Ca^{2+}-Piezo1 imaging involved incubating cells with Fluo-3 AM (2.5 µM) in HBSS buffer for 30 minutes
439 at 37˚C, followed by washing and imaging in RPMI containing 10% FBS, and 25 mM HEPES media.
440 Jurkat cell were transfected with Piezo1 mCherry plasmid and only those expressing Piezo1 mCherry

441 were selected for the study. Dual-colour sequential TIRF imaging was employed, with Piezo1 mCherry
442 being imaged at 300 ms (100 frames) and Ca2+ imaging performed using a 10 ms exposure time (2000
443 frames). The short exposure for Ca2+ was used to capture transient local peaks of fluorescence which
444 would otherwise average out at longer exposure times. The maximum projection of the time series
445 was used to detect local peaks using adaptive local thresholding (MATLAB), and a size filter was used
446 to exclude large objects identified with a relatively low Ca^{2+} gradient. For each specific set of settings,
447 the Ca^{2+} signal objects detected were used to calculate the average cluster size and total area of
448 objects. Uniform random numbers were used to simulate clusters with appropriate probability to
449 ensure that the final area of the simulated Ca^{2+} clusters closely matched the real data. The overlap
450 between the real Ca^{2+} signal and Piezo1 objects was compared with the simulated data to test for
451 deviation from a random placement of Ca^{2+} spots. To assess the robustness of the results, different
452 combinations of size filters of Piezo1 and Ca^{2+} objects were used, ranging from 50 to 350 pixels.

453 **Calpain Inhibition**

454 PD150606 (Merck, India), a non-competitive calpain 1 and 2 inhibitors, was used at a concentration of
455 100µM. Untransfected $CD4^+$ T lymphocytes were treated with PD150606 for 1 hour at 37°C prior to
456 treatment of chemokine. Post -chemokine treatment cells were stained either with pFAK as described.

457 **Focal adhesion kinase Inhibition**

458 FAK inhibitor 14 (1,2,4,5-Benzenetetraamine tetrahydrochloride) was used to selectively inhibit FAK
459 activity. Inhibitor was added at a final concentration 10µM, 1 hour prior to treatment with
460 recombinant CCL19. Post-treatment with CCL19, $CD4^+$ T lymphocytes were stained with Piezo1 for
461 confocal imaging.

462 **Piezo1 Inhibition**

463 Primary human $CD4^+$ T cells were incubated with 10µM of GsMTx4 for 1 hour prior to transwell
464 chemotaxis assay in response to recombinant CCL19.

465 **Statistics**

466 Student t-test was used to calculate significance.

467

468 **ACKNOWLEDGEMENTS**

The study was funded by Council of Scientific and Industrial Research, India (Grant no. FBR MLP-140). D.G. is a recipient of Swarnajayanti Fellowship from Department of Science and Technology, Government of India. The authors express their gratitude for provision of the Piezo1 constructs by Dr. Charles Cox, Victor Chang Institute of Cardiac Research, Australia.

The authors declare no competing interests

C.S.C.L. designed, performed and analyzed most of the experiments, prepared the figures and took part in writing the manuscript; T.M., B.S. and C.S.C.L. performed the IRM experiments; T.M. and B.S. analyzed IRM data; C.S.C.L., P.B. and D.K.S. performed image analyses; Pu.B., M.A.H., B.P.S., J.S. and R.D. helped with cell culture and confocal microscopy experiments; D.G. conceptualized and supervised the study, acquired funding, designed experiments and wrote the manuscript with input from all authors.

REFERENCES

1. Shechter R, London A, Schwartz M. Orchestrated leukocyte recruitment to immune-privileged sites: absolute barriers versus educational gates. Nat Rev Immunol. 2013 Mar;13(3):206-18. doi: 10.1038/nri3391.
2. Krummel MF, Bartumeus F, Gérard A. T cell migration, search strategies and mechanisms. Nat Rev Immunol. 2016 Mar;16(3):193-201. doi: 10.1038/nri.2015.16.
3. Woodland DL, Kohlmeier JE. Migration, maintenance and recall of memory T cells in peripheral tissues. Nat Rev Immunol. 2009 Mar;9(3):153-61. doi: 10.1038/nri2496.
4. Masopust D, Schenkel JM. The integration of T cell migration, differentiation and function. Nat Rev Immunol. 2013 May;13(5):309-20. doi: 10.1038/nri3442.
5. Fowell DJ, Kim M. The spatio-temporal control of effector T cell migration. Nat Rev Immunol. 2021 Sep;21(9):582-596. doi: 10.1038/s41577-021-00507-0.
6. Dupré L, Houmadi R, Tang C, Rey-Barroso J. T Lymphocyte Migration: An Action Movie Starring the Actin and Associated Actors. Front Immunol. 2015 Nov 18;6:586. doi: 10.3389/fimmu.2015.00586.
7. Nordenfelt P, Moore TI, Mehta SB, Kalappurakkal JM, Swaminathan V, Koga N, Lambert TJ, Baker D, Waters JC, Oldenbourg R, Tani T, Mayor S, Waterman CM, Springer TA. Direction of actin flow dictates integrin LFA-1 orientation during leukocyte migration. Nat Commun. 2017 Dec 11;8(1):2047. doi: 10.1038/s41467-017-01848-y.

500 8. Moreau HD, Piel M, Voituriez R, Lennon-Duménil AM. Integrating Physical and Molecular
501 Insights on Immune Cell Migration. Trends Immunol. 2018 Aug;39(8):632-643. doi:
502 10.1016/j.it.2018.04.007.
503 9. Shannon MJ, Pineau J, Griffié J, Aaron J, Peel T, Williamson DJ, Zamoyska R, Cope AP, Cornish
504 GH, Owen DM. Differential nanoscale organisation of LFA-1 modulates T-cell migration. J Cell
505 Sci. 2019 Oct 16;133(5):jcs232991. doi: 10.1242/jcs.232991.
506 10. Coste B, Mathur J, Schmidt M, Earley TJ, Ranade S, Petrus MJ, Dubin AE, Patapoutian A. Piezo1
507 and Piezo2 are essential components of distinct mechanically activated cation channels.
508 Science. 2010 Oct 1;330(6000):55-60. doi: 10.1126/science.1193270.
509 11. Coste B, Xiao B, Santos JS, Syeda R, Grandl J, Spencer KS, Kim SE, Schmidt M, Mathur J, Dubin
510 AE, Montal M, Patapoutian A. Piezo proteins are pore-forming subunits of mechanically
511 activated channels. Nature. 2012 Feb 19;483(7388):176-81. doi: 10.1038/nature10812.
512 12. Syeda R, Florendo MN, Cox CD, Kefauver JM, Santos JS, Martinac B, Patapoutian A. Piezo1
513 Channels Are Inherently Mechanosensitive. Cell Rep. 2016 Nov 8;17(7):1739-1746. doi:
514 10.1016/j.celrep.2016.10.033.
515 13. Murthy SE, Dubin AE, Patapoutian A. Piezos thrive under pressure: mechanically activated ion
516 channels in health and disease. Nat Rev Mol Cell Biol. 2017 Dec;18(12):771-783. doi:
517 10.1038/nrm.2017.92. Epub 2017 Oct 4. PMID: 28974772.
518 14. Liu CSC, Raychaudhuri D, Paul B, Chakrabarty Y, Ghosh AR, Rahaman O, Talukdar A, Ganguly
519 D. Cutting Edge: Piezo1 Mechanosensors Optimize Human T Cell Activation. J Immunol. 2018
520 Feb 15;200(4):1255-1260. doi: 10.4049/jimmunol.1701118.
521 15. Atcha H, Jairaman A, Holt JR, Meli VS, Nagalla RR, Veerasubramanian PK, Brumm KT, Lim HE,
522 Othy S, Cahalan MD, Pathak MM, Liu WF. Mechanically activated ion channel Piezo1
523 modulates macrophage polarization and stiffness sensing. Nat Commun. 2021 May
524 31;12(1):3256. doi: 10.1038/s41467-021-23482-5.
525 16. Geng J, Shi Y, Zhang J, Yang B, Wang P, Yuan W, Zhao H, Li J, Qin F, Hong L, Xie C, Deng X, Sun
526 Y, Wu C, Chen L, Zhou D. TLR4 signalling via Piezo1 engages and enhances the macrophage
527 mediated host response during bacterial infection. Nat Commun. 2021 Jun 10;12(1):3519. doi:
528 10.1038/s41467-021-23683-y.
529 17. Jairaman A, Othy S, Dynes JL, Yeromin AV, Zavala A, Greenberg ML, Nourse JL, Holt JR, Cahalan
530 SM, Marangoni F, Parker I, Pathak MM, Cahalan MD. Piezo1 channels restrain regulatory T
531 cells but are dispensable for effector CD4+ T cell responses. Sci Adv. 2021 Jul
532 7;7(28):eabg5859. doi: 10.1126/sciadv.abg5859.

533 **18.** Jäntti H, Sitnikova V, Ishchenko Y, Shakirzyanova A, Giudice L, Ugidos IF, Gómez-Budia M,
534 Korvenlaita N, Ohtonen S, Belaya I, Fazaludeen F, Mikhailov N, Gotkiewicz M, Ketola K,
535 Lehtonen Š, Koistinaho J, Kanninen KM, Hernández D, Pébay A, Giugno R, Korhonen P,
536 Giniatullin R, Malm T. Microglial amyloid beta clearance is driven by PIEZO1 channels. J
537 Neuroinflammation. 2022 Jun 15;19(1):147. doi: 10.1186/s12974-022-02486-y.
538 19. Liu CSC, Ganguly D. Mechanical Cues for T Cell Activation: Role of Piezo1 Mechanosensors.
539 Crit Rev Immunol. 2019;39(1):15-38. doi: 10.1615/CritRevImmunol.2019029595.
540 20. Ma S, Dubin AE, Zhang Y, Mousavi SAR, Wang Y, Coombs AM, Loud M, Andolfo I, Patapoutian
541 A. A role of PIEZO1 in iron metabolism in mice and humans. Cell. 2021 Feb 18;184(4):969-
542 982.e13. doi: 10.1016/j.cell.2021.01.024.
543 21. He Y, Deng B, Liu S, Luo S, Ning Y, Pan X, Wan R, Chen Y, Zhang Z, Jiang J, Xu H, Xia M, Li J.
544 Myeloid Piezo1 Deletion Protects Renal Fibrosis by Restraining Macrophage Infiltration and
545 Activation. Hypertension. 2022 May;79(5):918-931. doi:
546 10.1161/HYPERTENSIONAHA.121.18750.
547 22. Huang Z, Sun Z, Zhang X, Niu K, Wang Y, Zheng J, Li H, Liu Y. Loss of stretch-activated channels,
548 PIEZOs, accelerates non-small cell lung cancer progression and cell migration. Biosci Rep. 2019
549 Mar 22;39(3): BSR20181679. doi: 10.1042/BSR20181679.
550 23. Chubinskiy-Nadezhdin VI, Vasileva VY, Vassilieva IO, Sudarikova AV, Morachevskaya EA,
551 Negulyaev YA. Agonist-induced Piezo1 activation suppresses migration of transformed
552 fibroblasts. Biochem Biophys Res Commun. 2019 Jun 18;514(1):173-179. doi:
553 10.1016/j.bbrc.2019.04.139.
554 24. Mousawi F, Peng H, Li J, Ponnambalam S, Roger S, Zhao H, Yang X, Jiang LH. Chemical
555 activation of the Piezo1 channel drives mesenchymal stem cell migration via inducing ATP
556 release and activation of P2 receptor purinergic signaling. Stem Cells. 2020 Mar;38(3):410-
557 421. doi: 10.1002/stem.3114.
558 25. Wang X, Cheng G, Miao Y, Qiu F, Bai L, Gao Z, Huang Y, Dong L, Niu X, Wang X, Li Y, Tang H, Xu
559 Y, Song X. Piezo type mechanosensitive ion channel component 1 facilitates gastric cancer
560 omentum metastasis. J Cell Mol Med. 2021 Feb;25(4):2238-2253. doi: 10.1111/jcmm.16217.
561 26. Gao L, Ji Y, Wang L, He M, Yang X, Qiu Y, Sun X, Ji Z, Yang G, Zhang J, Li S, Dai L, Zhang L.
562 Suppression of Esophageal Squamous Cell Carcinoma Development by Mechanosensitive
563 Protein Piezo1 Downregulation. ACS Omega. 2021 Apr 12;6(15):10196-10206. doi:
564 10.1021/acsomega.1c00505.

565 27. Holt JR, Zeng WZ, Evans EL, Woo SH, Ma S, Abuwarda H, Loud M, Patapoutian A, Pathak MM.
566 Spatiotemporal dynamics of PIEZO1 localization controls keratinocyte migration during
567 wound healing. Elife. 2021 Sep 27;10:e65415. doi: 10.7554/eLife.65415.
568 28. Velasco-Estevez M, Koch N, Klejbor I, Caratis F, Rutkowska A. Mechanoreceptor Piezo1 Is
569 Downregulated in Multiple Sclerosis Brain and Is Involved in the Maturation and Migration of
570 Oligodendrocytes in vitro. Front Cell Neurosci. 2022 May 26;16:914985. doi:
571 10.3389/fncel.2022.914985.
572 29. Hung WC, Yang JR, Yankaskas CL, Wong BS, Wu PH, Pardo-Pastor C, Serra SA, Chiang MJ, Gu
573 Z, Wirtz D, Valverde MA, Yang JT, Zhang J, Konstantopoulos K. Confinement Sensing and Signal
574 Optimization via Piezo1/PKA and Myosin II Pathways. Cell Rep. 2016 May 17;15(7):1430-1441.
575 doi: 10.1016/j.celrep.2016.04.035.
576 30. McHugh BJ, Buttery R, Lad Y, Banks S, Haslett C, Sethi T. Integrin activation by Fam38A uses a
577 novel mechanism of R-Ras targeting to the endoplasmic reticulum. J Cell Sci. 2010 Jan 1;123(Pt
578 1):51-61. doi: 10.1242/jcs.056424.
579 31. Xiao B. 2020. Levering Mechanically Activated Piezo Channels for Potential Pharmacological
580 Intervention. Annu Rev PharmacolToxicol. 60:195-218. doi: 10.1146/annurev-pharmtox-
581 010919-023703.
582 32. Barr VA, Bunnell SC. Interference reflection microscopy. Curr Protoc Cell Biol. 2009 Dec;
583 Chapter 4: Unit 4.23. doi: 10.1002/0471143030.cb0423s45.
584 33. Chakraborty M, Mukherjee B, Nalinakshan N, Biswas A, Nayak RK, Sinha B. Effect of
585 heterogeneous substrate adhesivity of follower cells on speed and tension profile of leader
586 cells in primary keratocyte collective cell migration. Biol Open. 2022 Mar 15;11(3):bio058893.
587 doi: 10.1242/bio.058893.
588 34. Mitra SK, Hanson DA, Schlaepfer DD. Focal adhesion kinase: in command and control of cell
589 motility. Nat Rev Mol Cell Biol. 2005 Jan;6(1):56-68. doi: 10.1038/nrm1549.
590 35. Katoh K. FAK-Dependent Cell Motility and Cell Elongation. Cells. 2020 Jan 12;9(1):192. doi:
591 10.3390/cells9010192.
592 36. Yamashiro S, Watanabe N. A new link between the retrograde actin flow and focal adhesions.
593 J Biochem. 2014 Nov;156(5):239-48. doi: 10.1093/jb/mvu053.
594 37. Martino F, Perestrelo AR, Vinarský V, Pagliari S, Forte G. Cellular Mechanotransduction: From
595 Tension to Function. Front Physiol. 2018 Jul 5;9:824. doi: 10.3389/fphys.2018.00824.
596 38. Sánchez-Martín L, Sánchez-Sánchez N, Gutiérrez-López MD, Rojo AI, Vicente-Manzanares M,
597 Pérez-Alvarez MJ, Sánchez-Mateos P, Bustelo XR, Cuadrado A, Sánchez-Madrid F, Rodríguez-
598 Fernández JL, Cabañas C. Signaling through the leukocyte integrin LFA-1 in T cells induces a

599 transient activation of Rac-1 that is regulated by Vav and PI3K/Akt-1. J Biol Chem. 2004 Apr
600 16;279(16):16194-205. doi: 10.1074/jbc.M400905200.
601 39. Roy NH, Kim SHJ, Buffone A Jr, Blumenthal D, Huang B, Agarwal S, Schwartzberg PL, Hammer
602 DA, Burkhardt JK. LFA-1 signals to promote actin polymerization and upstream migration in T
603 cells. J Cell Sci. 2020 Sep 9;133(17):jcs248328. doi: 10.1242/jcs.248328.
604 40. Ganguly D. Can Piezo2 substitute Piezo1 function in the context of T cell-specific deletion in
605 mice? Sci Adv, e-Letter published Sep 8, 2021, in response to Jairaman A et al.,
606 41. Chang JE, Buechler MB, Gressier E, Turley SJ, Carroll MC. Mechanosensing by Peyer's patch
607 stroma regulates lymphocyte migration and mucosal antibody responses. Nat Immunol. 2019
608 Nov;20(11):1506-1516. doi: 10.1038/s41590-019-0505-z.
609 42. Chen X, Wanggou S, Bodalia A, Zhu M, Dong W, Fan JJ, Yin WC, Min HK, Hu M, Draghici D, Dou
610 W, Li F, Coutinho FJ, Whetstone H, Kushida MM, Dirks PB, Song Y, Hui CC, Sun Y, Wang LY, Li
611 X, Huang X. A Feedforward Mechanism Mediated by Mechanosensitive Ion Channel PIEZO1
612 and Tissue Mechanics Promotes Glioma Aggression. Neuron. 2018 Nov 21;100(4):799-815.e7.
613 43. Yao M, Tijore A, Cheng D, Li JV, Hariharan A, Martinac B, Tran Van Nhieu G, Cox CD, Sheetz M.
614 Force- and cell state-dependent recruitment of Piezo1 drives focal adhesion dynamics and
615 calcium entry. Sci Adv. 2022 Nov 11;8(45):eabo1461.
616 44. Roy NH, MacKay JL, Robertson TF, Hammer DA, Burkhardt JK. Crk adaptor proteins mediate
617 actin-dependent T cell migration and mechanosensing induced by the integrin LFA-1. Sci
618 Signal. 2018 Dec 11;11(560):eaat3178. doi: 10.1126/scisignal.aat3178.
619 45. Limozin L, Sengupta K. Quantitative reflection interference contrast microscopy (RICM) in soft
620 matter and cell adhesion. Chemphyschem. 2009 Nov 9;10(16):2752-68.
621 46. Biswas A, Alex A, Sinha B. Mapping Cell Membrane Fluctuations Reveals Their Active
622 Regulation and Transient Heterogeneities. Biophys J. 2017 Oct 17;113(8):1768-1781. doi:
623 10.1016/j.bpj.2017.08.041.
624 47. Biswas A, Kashyap P, Datta S, Sengupta T, Sinha B. Cholesterol Depletion by MβCD Enhances
625 Cell Membrane Tension and Its Variations-Reducing Integrity. Biophys J. 2019 Apr
626 23;116(8):1456-1468.
627 48. Shiba H, Noguchi H, Fournier JB. Monte Carlo study of the frame, fluctuation and internal
628 tensions of fluctuating membranes with fixed area. Soft Matter. 2016 Feb 28;12(8):2373-80.
629 doi: 10.1039/c5sm01900a.

630

631

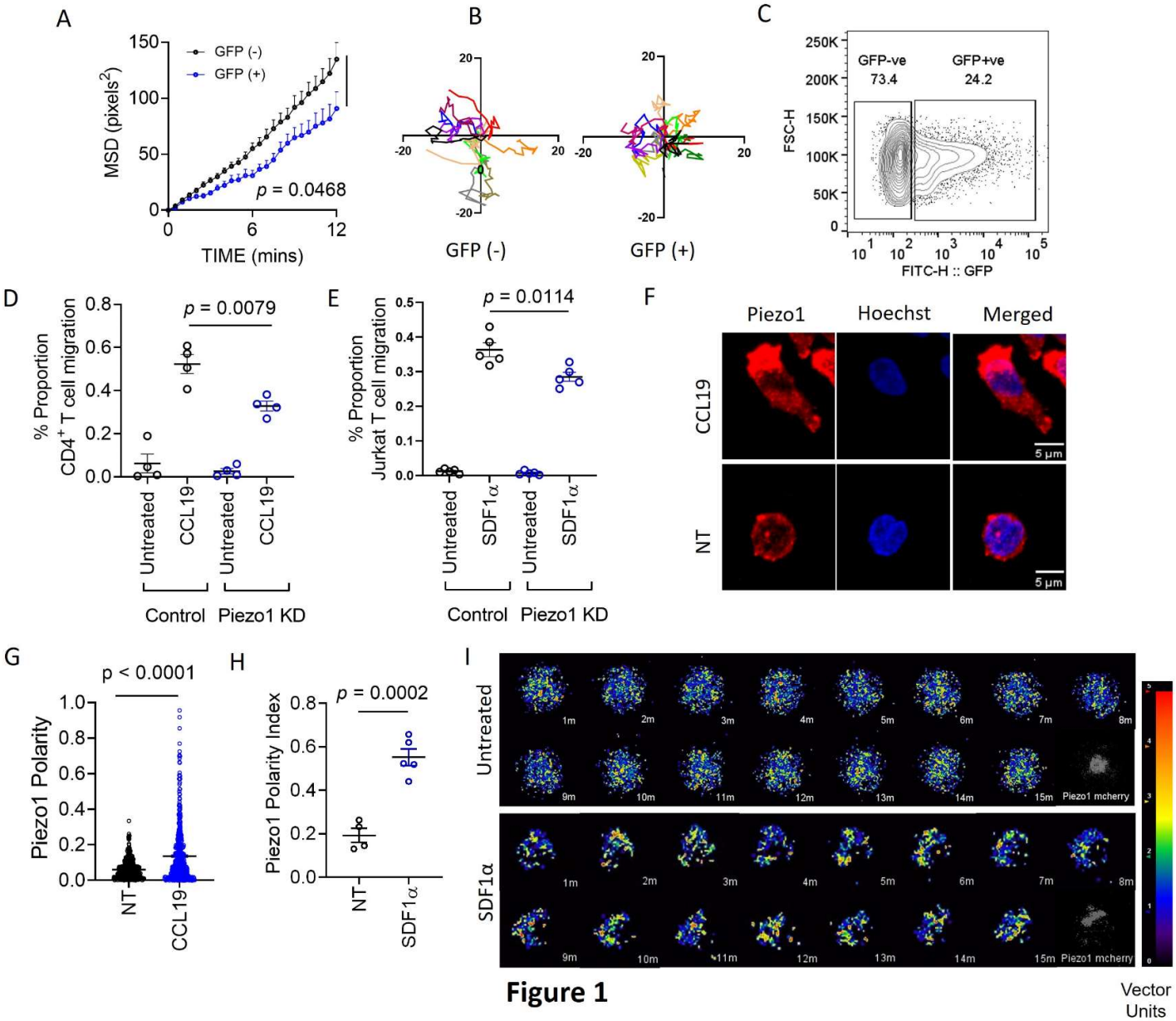

Figure 1

Figure 1. Piezo1 deficiency abrogates integrin-dependent motility in human T cells which is mediated through redistribution of Piezo1 at the leading edge in response to chemokine stimulation.

A. MSD versus time calculated for GFP⁺ (potential Piezo1-knockdown cells) and GFP⁻ (potential control cells) in GFP plasmid and Piezo1 siRNA co-transfected human CD4⁺ T lymphocytes, that were allowed to migrate in presence of recombinant CCL19 on ICAM1-coated dishes. **B.** Representative tracks of GFP⁺ and GFP⁻ CD4⁺ T lymphocytes. Comparisons of **C.** % GFP⁺ cells after 72 hours of nucleofection **D**

640 **& E.** 3D transwell migration assay of siRNA-transfected primary human $CD4^+$ T lymphocytes (D) and
641 Jurkat T cells (E), respectively. Data representative of at least 3 independent experiments. **F.**
642 Representative confocal images of Piezo1 distribution in fixed untreated and CCL19-treated $CD4^+$ T
643 lymphocytes. 63X oil magnification. **G.** Comparison between Piezo1 polarity index calculated for fixed,
644 stained, human $CD4^+$ T lymphocytes with or without 0.5µg/ml CCL19 treatment for 20-30 minutes. n
645 > 510 random cells, each. **H.** Piezo1 polarity index calculated for Jurkat cells, expressing mCherry-
646 tagged Piezo1 during live-cell tracking in the presence of recombinant SDF1α. Each dot represents
647 polarity index of each cell, averaged over all the time-frames. **I.** Representative time kinetics of particle
648 image velocimetry (PIV) analysis of Piezo1-mcherry transfected Jurkat cells, allowed to move on ICAM-
649 coated dishes in the presence of recombinant SDF1α. Top panel: No chemokine. Bottom Panel: SDF1α.

650

651

652

653

654

655

656

657

658

659

660

661

662

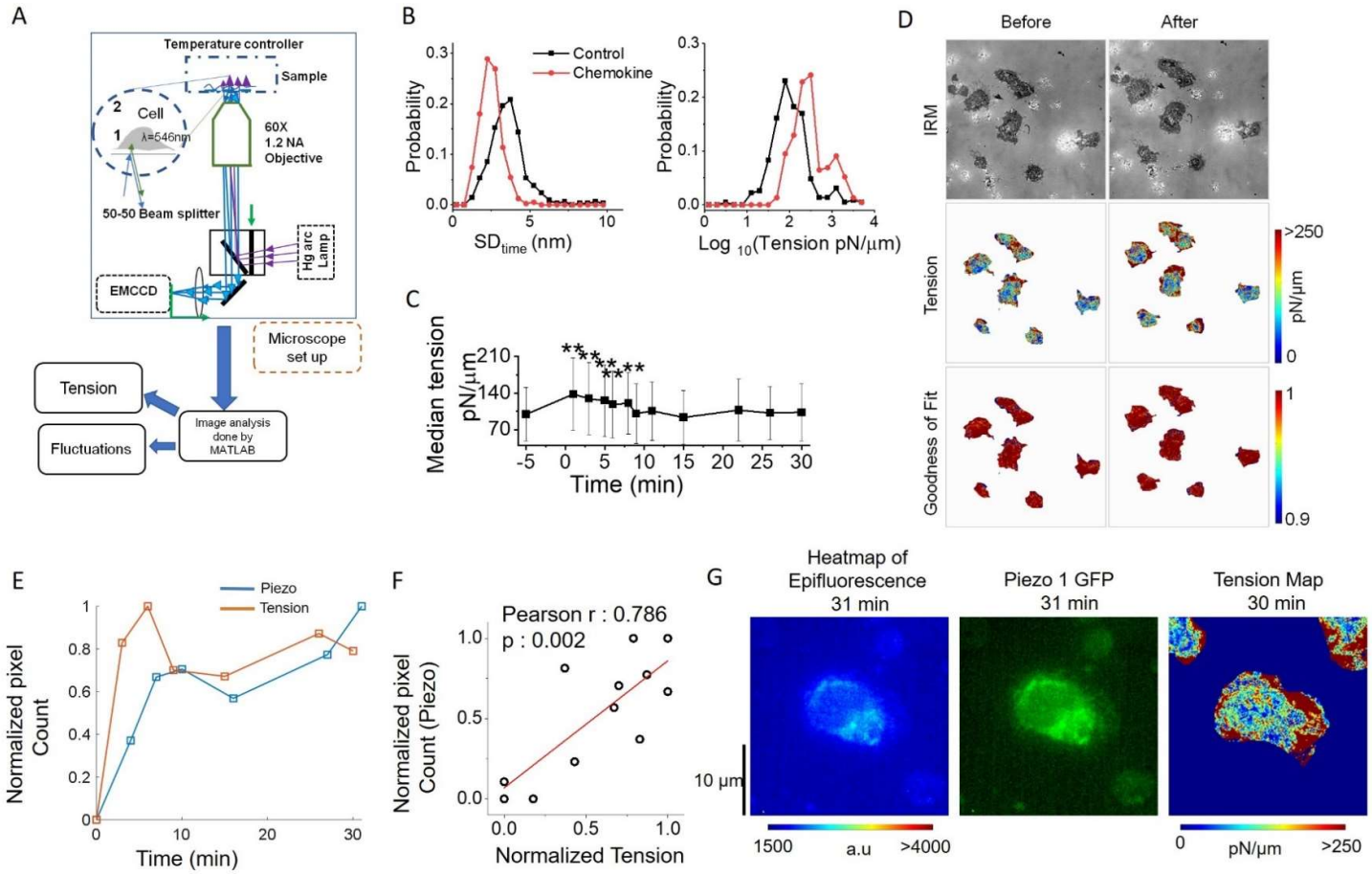

Figure 2

Figure 2. Piezo1 redistribution in migrating T cells follow increased membrane tension in the leading edge

A. Schematic illustration of interference reflection microscopy imaging setup. **B.** Probability distribution of amplitude of temporal fluctuations (SD_{time}, left) and tension (right) before and after addition of chemokines. **C.** Temporal trajectory of tension of cells before and after addition of chemokine with ** indicating significant difference from control. **D.** Representative IRM images of Jurkat cells (top), corresponding tension maps (middle) and R^2 maps (bottom), before and after chemokine treatment. **E** Correlation between normalized Piezo intensity, tension magnitudes with time. **F.** Scatter plot to show correlation between normalized pixel count of Piezo1 and normalized tension. Piezo1 intensity at specific time-points were correlated with tension magnitudes at the preceding timepoints. Normalization has been done such that the maximum value is set to 1 and others are accordingly scaled. **G.** Colour-coded Piezo1-GFP intensity map (left), epifluorescence image (middle), and tension map (right) of representative Piezo1-GFP expressing Jurkat cell, after 30 minutes of 0.1μg/ml of SDF1α treatment.

678

679

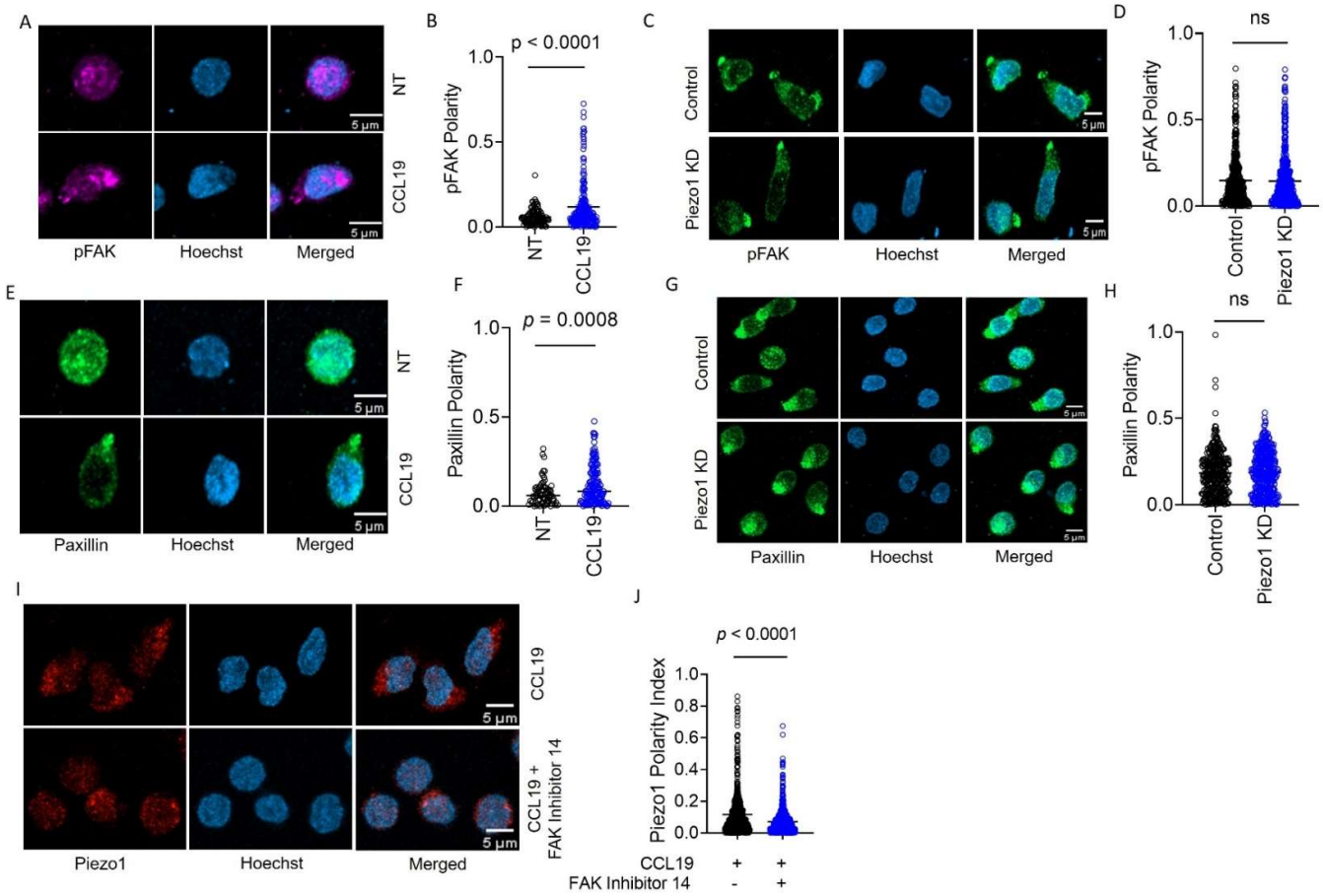

Figure 3

680

681 **Figure 3. Focal adhesion following chemokine receptor activation does not depend on Piezo1**

682 **A.** Representative confocal images of human CD4⁺ T lymphocytes, fixed and stained for phospho-FAK
683 (pFAK) under untreated and CCL19-treated conditions. **B.** Increased polarity of pFAK upon chemokine
684 stimulation of CD4⁺ T lymphocytes as compared to unstimulated controls. N > 120 cells, each. **C.**
685 Representative confocal images of pFAK distribution in control and Piezo1 siRNA-transfected CD4⁺ T
686 lymphocytes stimulated with chemokine. **D**. Comparison of pFAK polarity in CCL19-stimulated control
687 and Piezo1-knockdown CD4⁺ T lymphocytes. n > 450 random cells, each. **E.** Representative confocal
688 images of paxillin distribution in untreated versus CCL19-stimulated CD4⁺ T lymphocytes. **F.** Increased
689 paxillin polarity in response to CCL19 stimulation as compared to untreated CD4⁺ T lymphocytes.
690 Untreated n > 70, CCL19-treated n > 150. **G.** Representative confocal images of immunostained paxillin
691 in chemokine-stimulated, control and Piezo1-knockdown CD4⁺ T lymphocytes. **H**. Comparison of
692 paxillin polarity in CCL19-stimulated control and Piezo1-knockdown CD4⁺ T lymphocytes. n > 550
693 random cells, each. **I.** Representative confocal images of stained Piezo1 in CD4⁺ T cells stimulated with

694 CCL19 in the presence or absence of FAK inhibitor 14. **J.** Effect of FAK inhibition on Piezo1 polarity in
695 $CD4^+$ T lymphocytes stimulated with recombinant CCL19 versus untreated cells. n > 600 random cells,
696 each. Data represented from at least 3 independent experiments.

697

698

699

700

701

702

703

704

705

706

707

708

709

710

711

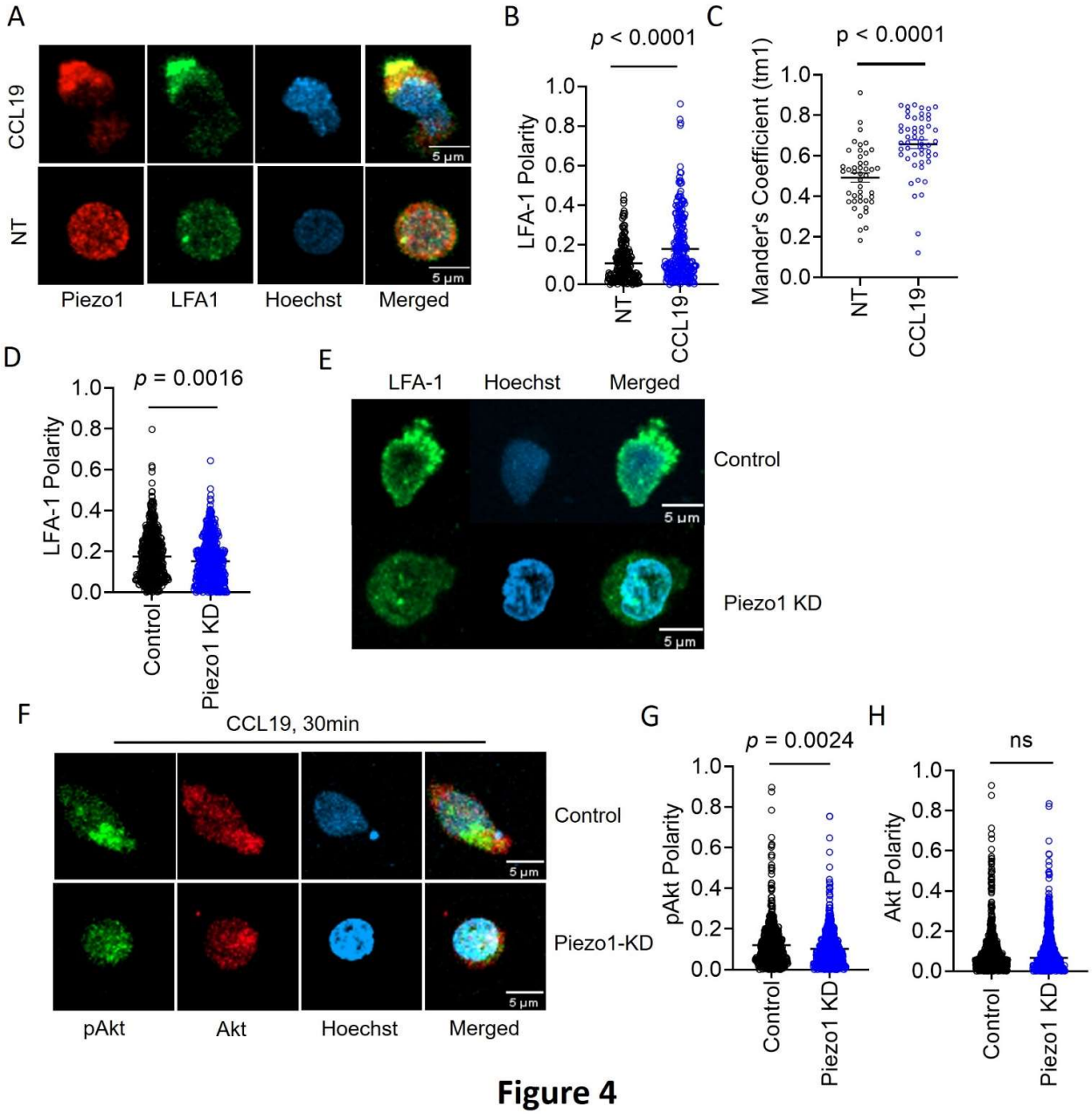

Figure 4

Figure 4. Membrane recruitment of LFA1 on chemokine receptor activation disrupts with Piezo1 deficiency.

A. Representative confocal images of fixed, immunostained Piezo1 and LFA1 in unstimulated and CCL19-stimulated $CD4^+$ T lymphocytes. **B.** Increased LFA1 polarity in response to recombinant CCL19 stimulation in $CD4^+$ T cells. n > 295 random cells, each. **C.** Manders' co-localisation analysis of Piezo1 and LFA1 in untreated and CCL19-treated $CD4^+$ T lymphocytes. **D.** Comparison of LFA1 polarity in chemokine-treated control and Piezo1 knockdown $CD4^+$ T lymphocytes. **E.** Representative confocal stained images of LFA1 polarity of CCL19-treated control and Piezo1-knockdown $CD4^+$ T lymphocytes. n > 490 random cells, each. **F.** Representative confocal images of phospho-Akt (pAkt) and Akt

721 distribution upon chemokine treatment of control and Piezo1-knockdown cells. **G & H.** Quantitative
722 analyses of pAkt (M) and Akt (N) polarity in control and Piezo1-knockdown cells after CCL19-
723 treatment. n > 580 random cells, each. Data represented from at least 3 independent experiments.

724

725

726

727

728

729

730

731

732

733

734

735

736

737

738

739

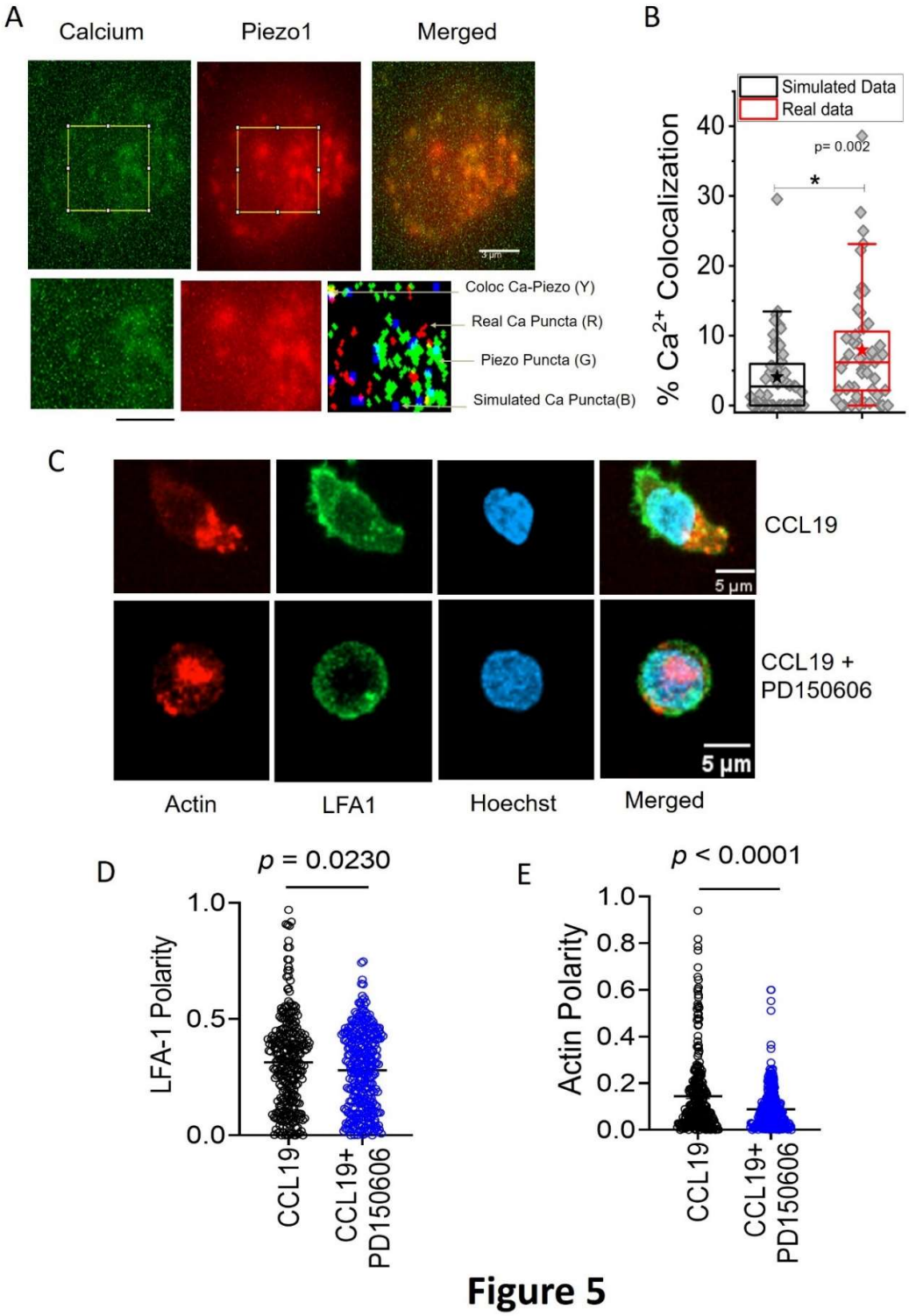

Figure 5

Figure 5. Local Ca^{2+} mobilization with Piezo1 redistribution upon chemokine stimulation.

A. Representative TIRF image of a Jurkat Cell stained with Fluo3AM and transiently expressing with Piezo1 mCherry. Lower panel: zoomed in image and overlap of binary images of objects detected from

743 Calcium and Piezo channels as well as simulated randomly placed punctas having similar total (in the
744 zoomed in section) and average area as that of the Calcium punctas detected in the real images.
745 Overlap RGB image shows the overlap between Real Calcium (Red) and piezo puncta (Green), overlap
746 puncta (Yellow), simulated calcium puncta (blue). **B.** Comparison between percentage calcium
747 colocalization of simulated data and real data. * Denote p value < 0.05 calculated using Mann Whitney
748 U test. N cell= 52 (13 cells x 4 time points). NROIS= 52. **C.** Representative confocal images of LFA1 and
749 actin distribution in CCL19-stimulated CD4+ T lymphocytes with or without inhibition of calpain.
750 100µM of PD15606 was added to the cells 1 hour prior to addition of chemokine. Quantitative
751 comparisons of **D.** LFA1 and **E.** actin polarity upon chemokine stimulation, in the presence or absence
752 of calpain pre-inhibition. N > 290 random cells, each. Data represented is of at least 3 independent
753 experiments.

754

755

756

757

758

759

760

761

762

763

764

765

766

767

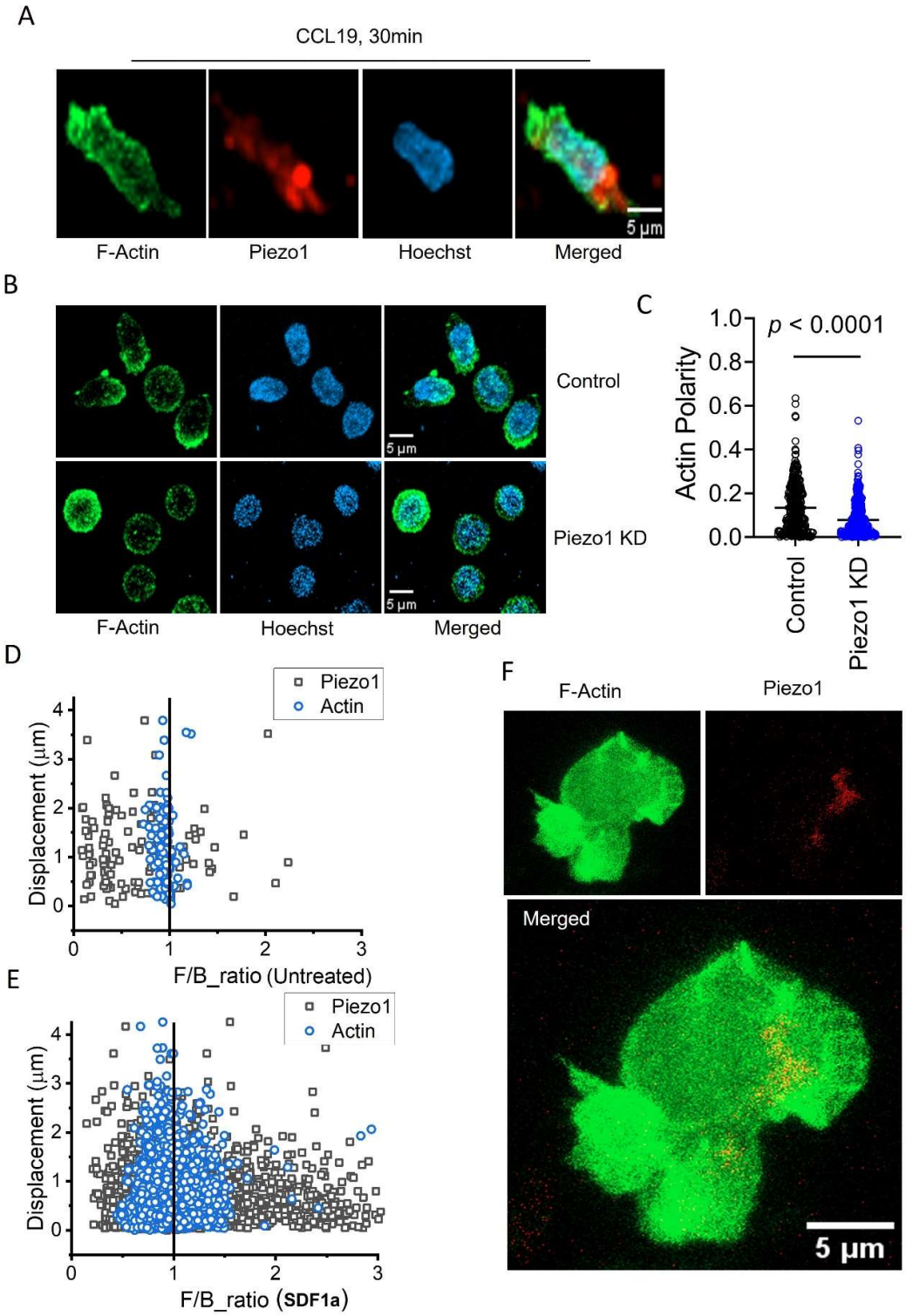

Figure 6

768 **Figure 6. Piezo1 deficiency disrupts F-actin retrograde flow in T cells despite chemokine receptor**
769 **activation.**

770 **A.** Representative fixed confocal images of actin and Piezo1 distribution in $CD4^+$ T lymphocytes after
771 30 mins of 0.5µg/ml recombinant CCL19 treatment. **B.** Quantitative comparison of actin polarity in
772 control and Piezo1-knockdown $CD4^+$ T lymphocytes cells after 30 mins of chemokine treatment. n >
773 300 random cells, each. **C.** Representative fixed confocal images of actin distribution in chemokine-
774 treated, control and Piezo1-knockdown $CD4^+$ T lymphocytes. Front-back (F/B) of Piezo1 and actin-GFP
775 in SDF1α treated **(D)** and untreated **(E)** Jurkat cells co-expressing actin-GFP and Piezo1-mCherry. **F.** A
776 snapshot of time-lapse imaging of Piezo1-mCherry and actin-GFP expressing Jurkat cell treated with
777 0.1µg/ml of SDF1α. Image is maximum Z-projection of the cell at 63X/1.40 magnification. Data
778 represented is of at least 3 independent experiments.

779

780

781

782

783

784

785

786

787

788

789

790

791

792

793

794

795

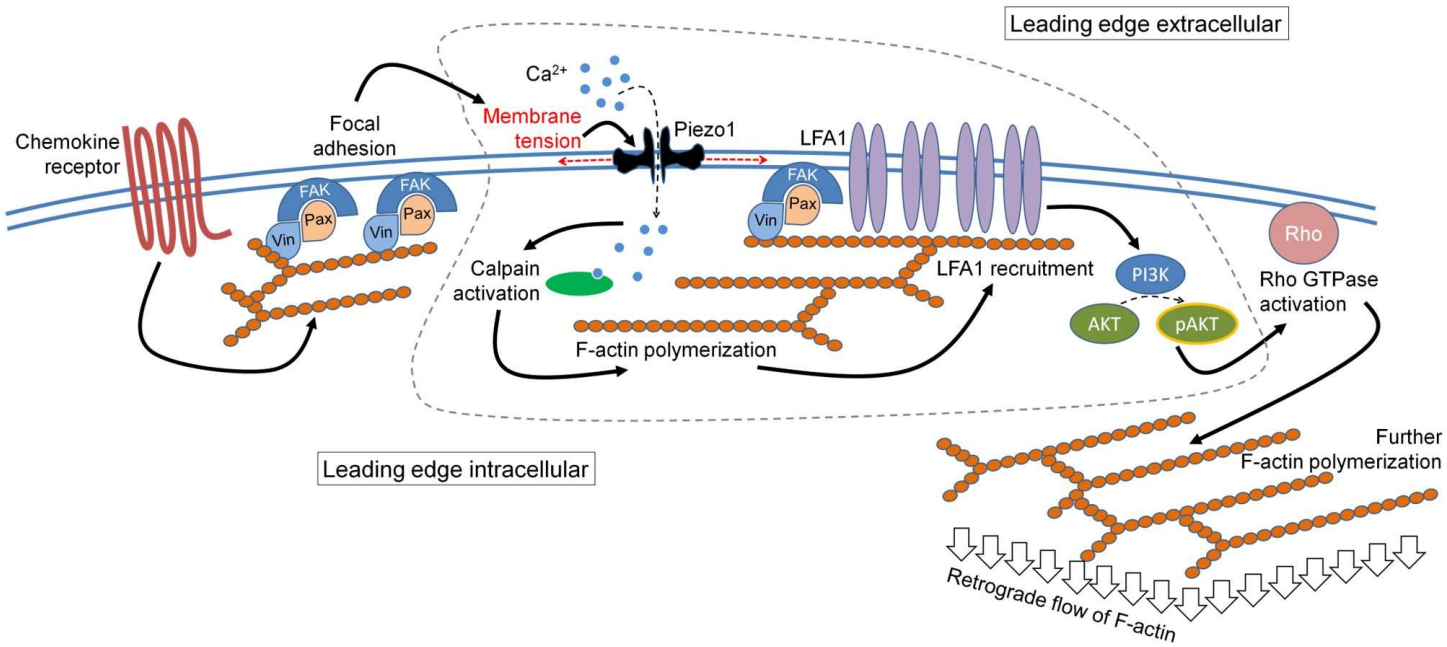

Figure 7

The mechanistic model depicting involvement of Piezo1 mechanosensing in leading edge events in a migrating T cell.

Proposed model suggests chemokine receptor activation in human T cells lead to focal adhesion kinase activation and focal adhesion formation. Focal adhesions lead to localized increase in membrane tension at the leading edge plasma membrane which leads to Piezo1 recruitment and activation. Piezo1 activation leads to calpain activation which potentially drives further cytoskeletal consolidation to recruit integrin LFA1. LFA1 recruitment and activation lead to phosphorylation of AKT and downstream signaling eventually driving the retrograde actin flow in migrating human T cells.

808 **FIGURE LEGENDS**

809 **Figure 1. Piezo1 deficiency abrogates integrin-dependent motility in human T cells which is**
810 **mediated through redistribution of Piezo1 at the leading edge in response to chemokine**
811 **stimulation.**

812 **A.** MSD versus time calculated for GFP^+ (potential Piezo1-knockdown cells) and GFP^- (potential control
813 cells) in GFP plasmid and Piezo1 siRNA co-transfected human $CD4^+$ T lymphocytes, that were allowed
814 to migrate in presence of recombinant CCL19 on ICAM1-coated dishes. **B.** Representative tracks of
815 GFP^+ and GFP^- $CD4^+$ T lymphocytes. Comparisons of **C.** % GFP^+ cells after 72 hours of nucleofection **D**
816 **& E.** 3D transwell migration assay of siRNA-transfected primary human $CD4^+$ T lymphocytes (D) and
817 Jurkat T cells (E), respectively. Data representative of at least 3 independent experiments. **F.**
818 Representative confocal images of Piezo1 distribution in fixed untreated and CCL19-treated $CD4^+$ T
819 lymphocytes. 63X oil magnification. **G.** Comparison between Piezo1 polarity index calculated for fixed,
820 stained, human $CD4^+$ T lymphocytes with or without 0.5µg/ml CCL19 treatment for 20-30 minutes. n
821 > 510 random cells, each. **H.** Piezo1 polarity index calculated for Jurkat cells, expressing mCherry-
822 tagged Piezo1 during live-cell tracking in the presence of recombinant SDF1α. Each dot represents
823 polarity index of each cell, averaged over all the time-frames. **I.** Representative time kinetics of particle
824 image velocimetry (PIV) analysis of Piezo1-mcherry transfected Jurkat cells, allowed to move on ICAM-
825 coated dishes in the presence of recombinant SDF1α. Top panel: No chemokine. Bottom Panel: SDF1α.

826

827 **Figure 2. Piezo1 redistribution in migrating T cells follow increased membrane tension in the leading**
828 **edge**

829 **A.** Schematic illustration of interference reflection microscopy imaging setup. **B.** Probability
830 distribution of amplitude of temporal fluctuations (SD_{time}, left) and tension (right) before and after
831 addition of chemokines. **C.** Temporal trajectory of tension of cells before and after addition of
832 chemokine with ** indicating significant difference from control. **D.** Representative IRM images of
833 Jurkat cells (top), corresponding tension maps (middle) and R^2 maps (bottom), before and after
834 chemokine treatment. **E** Correlation between normalized Piezo intensity, tension magnitudes with
835 time. **F.** Scatter plot to show correlation between normalized pixel count of Piezo1 and normalized
836 tension. Piezo1 intensity at specific time-points were correlated with tension magnitudes at the
837 preceding timepoints. Normalization has been done such that the maximum value is set to 1 and
838 others are accordingly scaled. **G.** Colour-coded Piezo1-GFP intensity map (left), epifluorescence image

839 (middle), and tension map (right) of representative Piezo1-GFP expressing Jurkat cell, after 30 minutes
840 of 0.1μg/ml of SDF1α treatment.

841

842 **Figure 3. Focal adhesion following chemokine receptor activation does not depend on Piezo1**

843 **A.** Representative confocal images of human $CD4^+$ T lymphocytes, fixed and stained for phospho-FAK
844 (pFAK) under untreated and CCL19-treated conditions. **B.** Increased polarity of pFAK upon chemokine
845 stimulation of $CD4^+$ T lymphocytes as compared to unstimulated controls. N > 120 cells, each. **C.**
846 Representative confocal images of pFAK distribution in control and Piezo1 siRNA-transfected $CD4^+$ T
847 lymphocytes stimulated with chemokine. **D**. Comparison of pFAK polarity in CCL19-stimulated control
848 and Piezo1-knockdown $CD4^+$ T lymphocytes. n > 450 random cells, each. **E.** Representative confocal
849 images of paxillin distribution in untreated versus CCL19-stimulated $CD4^+$ T lymphocytes. **F.** Increased
850 paxillin polarity in response to CCL19 stimulation as compared to untreated $CD4^+$ T lymphocytes.
851 Untreated n > 70, CCL19-treated n > 150. **G.** Representative confocal images of immunostained paxillin
852 in chemokine-stimulated, control and Piezo1-knockdown $CD4^+$ T lymphocytes. **H**. Comparison of
853 paxillin polarity in CCL19-stimulated control and Piezo1-knockdown $CD4^+$ T lymphocytes. n > 550
854 random cells, each. **I.** Representative confocal images of stained Piezo1 in $CD4^+$ T cells stimulated with
855 CCL19 in the presence or absence of FAK inhibitor 14. **J.** Effect of FAK inhibition on Piezo1 polarity in
856 $CD4^+$ T lymphocytes stimulated with recombinant CCL19 versus untreated cells. n > 600 random cells,
857 each. Data represented from at least 3 independent experiments.

858

859 **Figure 4. Membrane recruitment of LFA1 on chemokine receptor activation disrupts with Piezo1**
860 **deficiency.**

861 **A.** Representative confocal images of fixed, immunostained Piezo1 and LFA1 in unstimulated and
862 CCL19-stimulated $CD4^+$ T lymphocytes. **B.** Increased LFA1 polarity in response to recombinant CCL19
863 stimulation in $CD4^+$ T cells. n > 295 random cells, each. **C.** Manders' co-localisation analysis of Piezo1
864 and LFA1 in untreated and CCL19-treated $CD4^+$ T lymphocytes. **D.** Comparison of LFA1 polarity in
865 chemokine-treated control and Piezo1 knockdown $CD4^+$ T lymphocytes. **E.** Representative confocal
866 stained images of LFA1 polarity of CCL19-treated control and Piezo1-knockdown $CD4^+$ T lymphocytes.
867 n > 490 random cells, each. **F.** Representative confocal images of phospho-Akt (pAkt) and Akt
868 distribution upon chemokine treatment of control and Piezo1-knockdown cells. **G & H.** Quantitative
869 analyses of pAkt (M) and Akt (N) polarity in control and Piezo1-knockdown cells after CCL19-
870 treatment. n > 580 random cells, each. Data represented from at least 3 independent experiments.

871

872 **Figure 5. Local Ca^{2+} mobilization with Piezo1 redistribution upon chemokine stimulation.**

873 **A.** Representative TIRF image of a Jurkat Cell stained with Fluo3AM and transiently expressing with
874 Piezo1 mCherry. Lower panel: zoomed in image and overlap of binary images of objects detected from
875 Calcium and Piezo channels as well as simulated randomly placed punctas having similar total (in the
876 zoomed in section) and average area as that of the Calcium punctas detected in the real images.
877 Overlap RGB image shows the overlap between Real Calcium (Red) and piezo puncta (Green), overlap
878 puncta (Yellow), simulated calcium puncta (blue). **B.** Comparison between percentage calcium
879 colocalization of simulated data and real data. * Denote p value < 0.05 calculated using Mann Whitney
880 U test. N cell= 52 (13 cells x 4 time points). NROIS= 52. **C.** Representative confocal images of LFA1 and
881 actin distribution in CCL19-stimulated CD4+ T lymphocytes with or without inhibition of calpain.
882 100µM of PD15606 was added to the cells 1 hour prior to addition of chemokine. Quantitative
883 comparisons of **D.** LFA1 and **E.** actin polarity upon chemokine stimulation, in the presence or absence
884 of calpain pre-inhibition. N > 290 random cells, each. Data represented is of at least 3 independent
885 experiments.

886

887 **Figure 6. Piezo1 deficiency disrupts F-actin retrograde flow in T cells despite chemokine receptor**
888 **activation.**

889 **A.** Representative fixed confocal images of actin and Piezo1 distribution in $CD4^+$ T lymphocytes after
890 30 mins of 0.5µg/ml recombinant CCL19 treatment. **B.** Quantitative comparison of actin polarity in
891 control and Piezo1-knockdown $CD4^+$ T lymphocytes cells after 30 mins of chemokine treatment. n >
892 300 random cells, each. **C.** Representative fixed confocal images of actin distribution in chemokine-
893 treated, control and Piezo1-knockdown $CD4^+$ T lymphocytes. Front-back (F/B) of Piezo1 and actin-GFP
894 in SDF1α treated **(D)** and untreated **(E)** Jurkat cells co-expressing actin-GFP and Piezo1-mCherry. **F.** A
895 snapshot of time-lapse imaging of Piezo1-mCherry and actin-GFP expressing Jurkat cell treated with
896 0.1µg/ml of SDF1α. Image is maximum Z-projection of the cell at 63X/1.40 magnification. Data
897 represented is of at least 3 independent experiments.

898

899 **Figure 7. The mechanistic model depicting involvement of Piezo1 mechanosensing in leading edge**
900 **events in a migrating T cell.**

901 Proposed model suggests chemokine receptor activation in human T cells lead to focal adhesion kinase
902 activation and focal adhesion formation. Focal adhesions lead to localized increase in membrane
903 tension at the leading edge plasma membrane which leads to Piezo1 recruitment and activation.
904 Piezo1 activation leads to calpain activation which potentially drives further cytoskeletal consolidation
905 to recruit integrin LFA1. LFA1 recruitment and activation lead to phosphorylation of AKT and
906 downstream signaling eventually driving the retrograde actin flow in migrating human T cells.

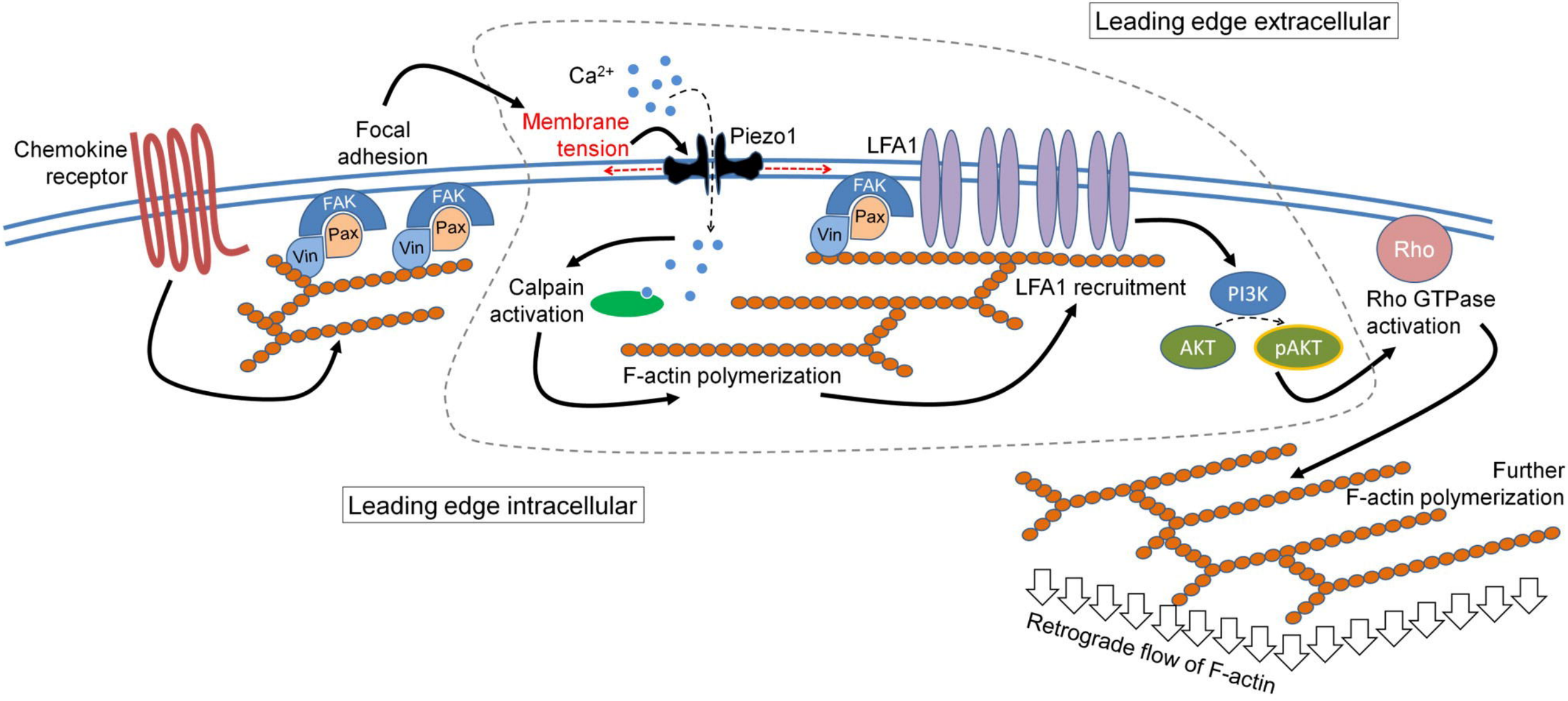
Leading edge extracellular
Ca2+
Chemokine receptor
Focal adhesion
Membrane tension
Piezo1
LFA1
FAK
Pax
Vin
FAK
Pax
Vin
FAK
Pax
Vin
Rho
Calpain activation
LFA1 recruitment
PI3K
Rho GTPase activation
AKT
pAKT
F-actin polymerization
Leading edge intracellular
Further F-actin polymerization
Retrograde flow of F-actin

Figure 7

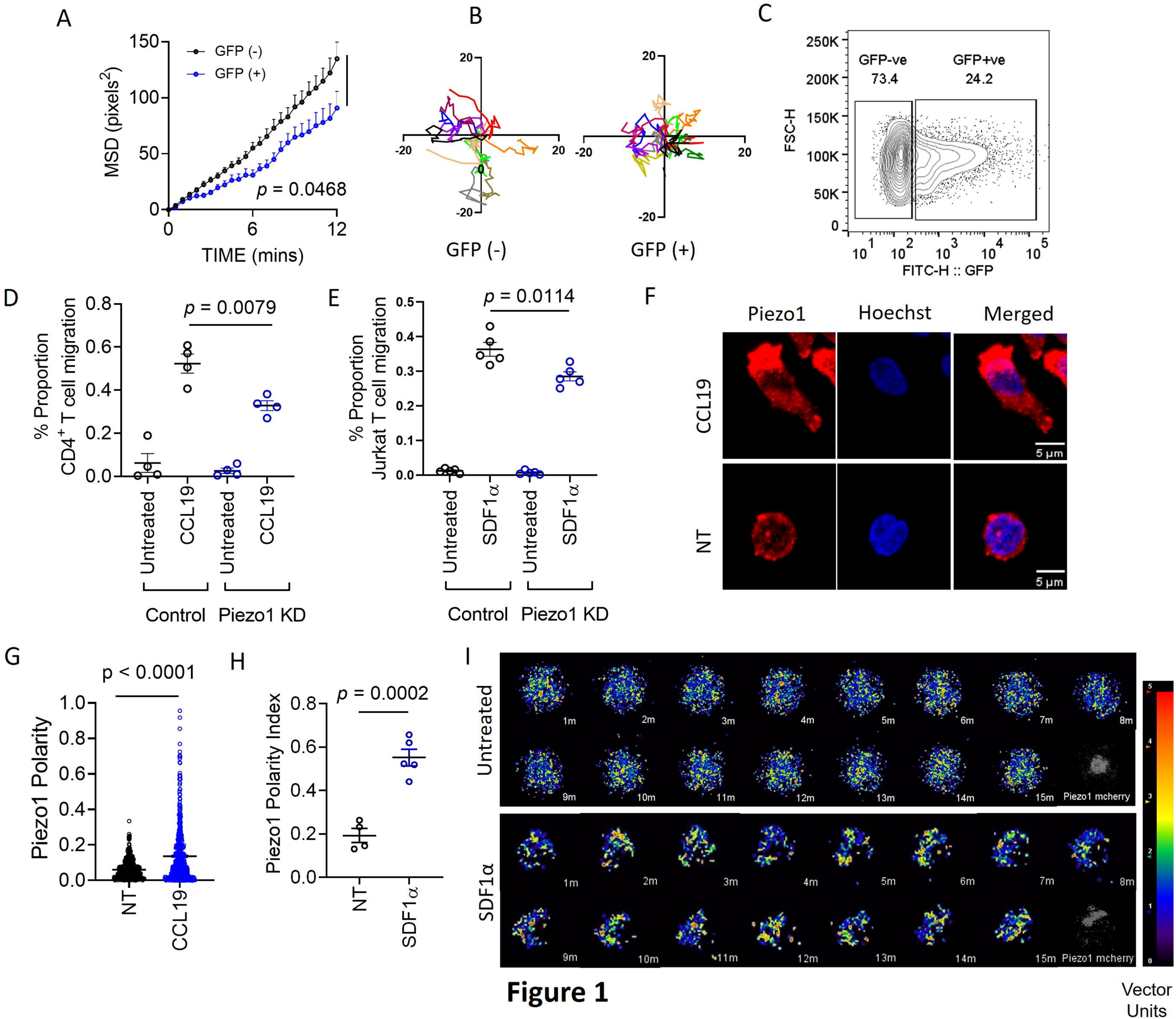
A
MSD (pixels^2)
GFP (-)
GFP (+)
p = 0.0468
TIME (mins)
B
GFP (-)
GFP (+)
C
GFP-ve
73.4
GFP+ve
24.2
FSC-H
FITC-H :: GFP
D
% Proportion CD4$^+$ T cell migration
p = 0.0079
Untreated
CCL19
Control
Piezo1 KD
E
% Proportion Jurkat T cell migration
p = 0.0114
Untreated
SDF1α
Control
Piezo1 KD
F
Piezo1
Hoechst
Merged
CCL19
NT
5 µm
G
Piezo1 Polarity
p < 0.0001
NT
CCL19
H
Piezo1 Polarity Index
p = 0.0002
NT
SDF1α
I
Untreated
SDF1α
1m
2m
3m
4m
5m
6m
7m
8m
9m
10m
11m
12m
13m
14m
15m
Piezo1 mcherry
Vector Units

Figure 1

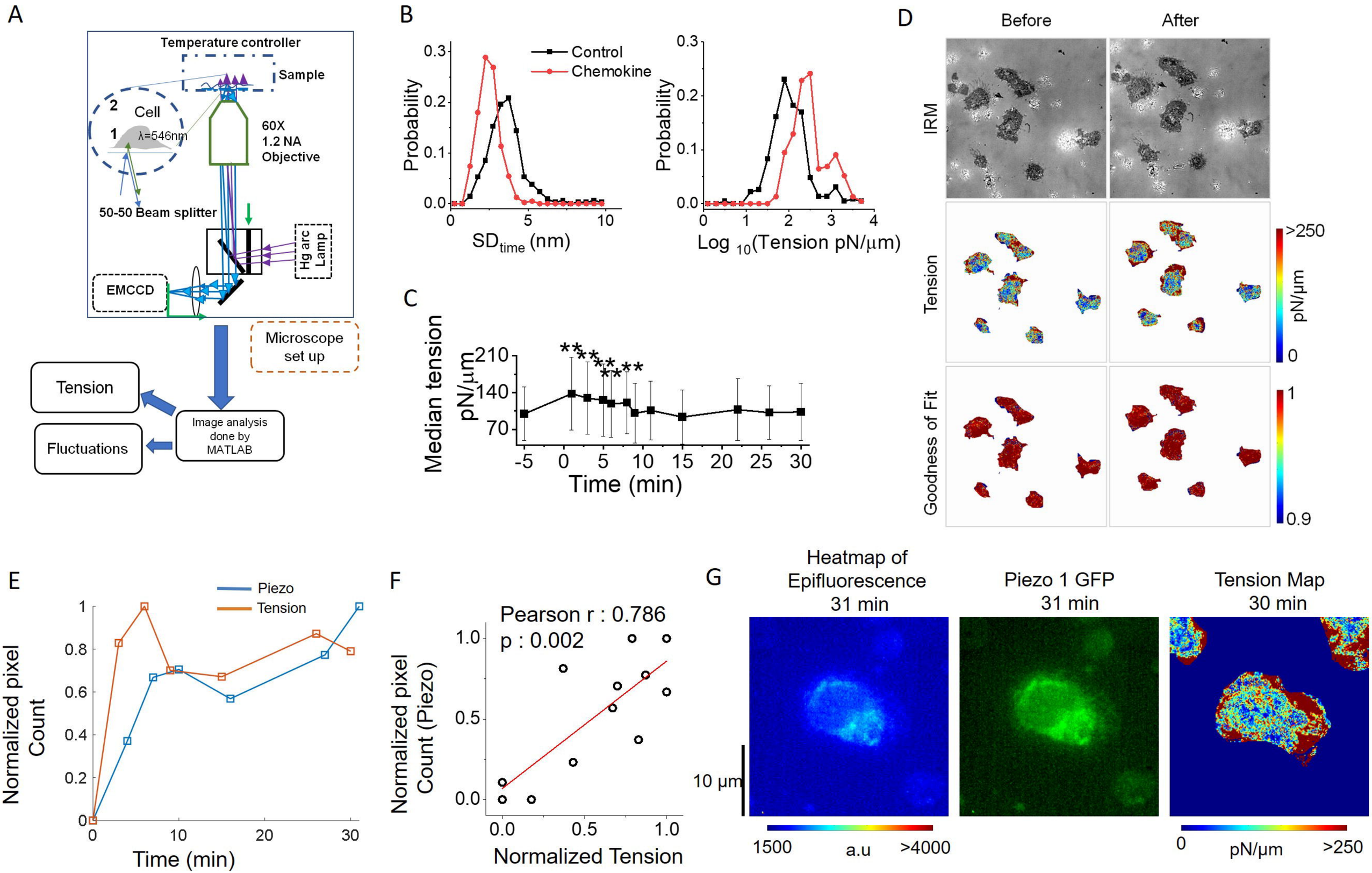
A
Temperature controller
Sample
Cell
2
1
λ=546nm
60X
1.2 NA
Objective
50-50 Beam splitter
Hg arc Lamp
EMCCD
Microscope set up
Tension
Fluctuations
Image analysis done by MATLAB
B
Control
Chemokine
Probability
SD time (nm)
Log 10(Tension pN/μm)
C
Median tension pN/μm
Time (min)
D
Before
After
IRM
Tension
Goodness of Fit
>250
pN/μm
0
1
0.9
E
Piezo
Tension
Normalized pixel Count
Time (min)
F
Pearson r : 0.786
p : 0.002
Normalized pixel Count (Piezo)
Normalized Tension
G
Heatmap of Epifluorescence 31 min
Piezo 1 GFP 31 min
Tension Map 30 min
10 μm
1500
a.u
>4000
0
pN/μm
>250

Figure 2

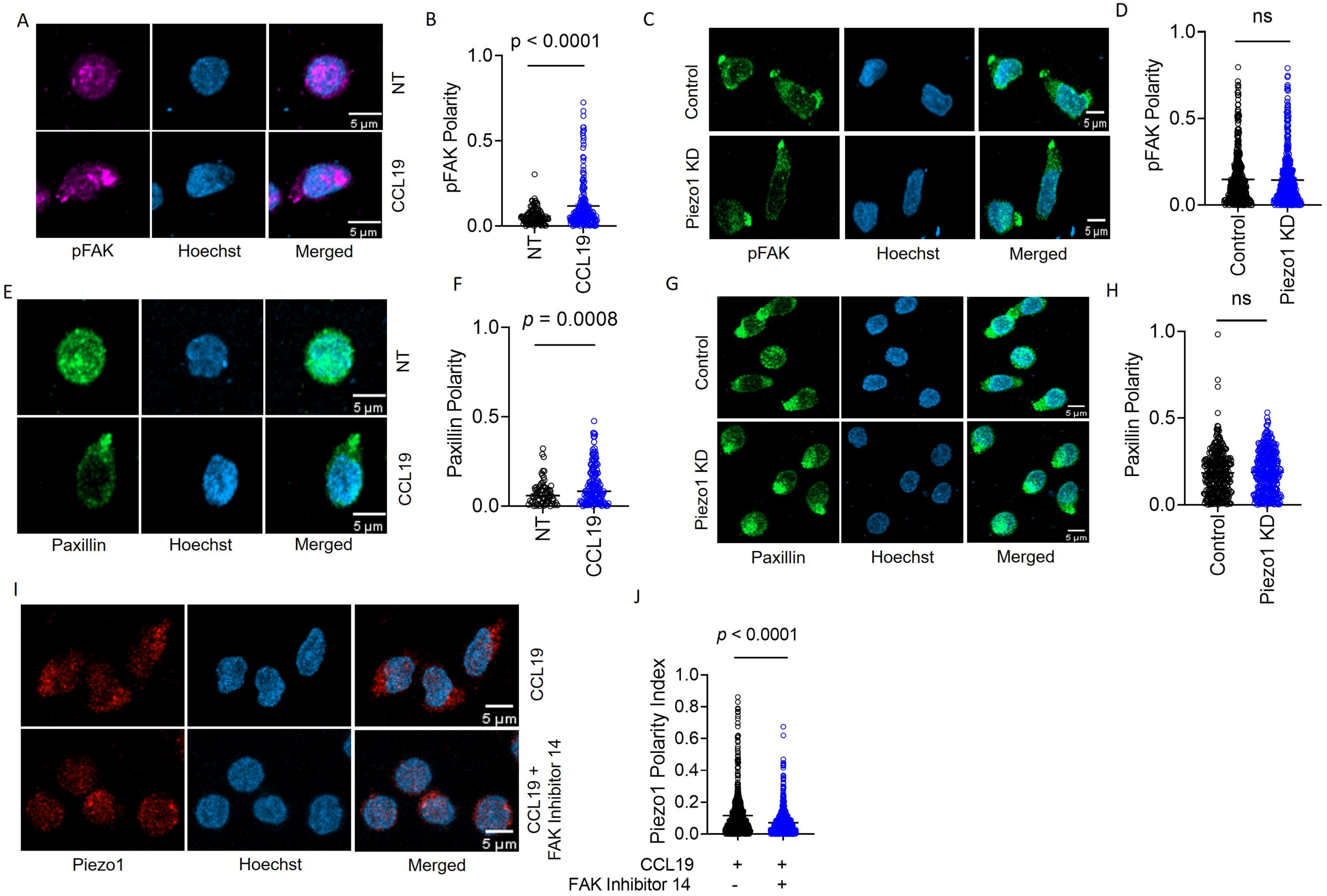
A
NT
CCL19
5 µm
pFAK
Hoechst
Merged
B
p < 0.0001
pFAK Polarity
1.0
0.5
0.0
NT
CCL19
C
Control
Piezo1 KD
5 µm
pFAK
Hoechst
Merged
D
ns
pFAK Polarity
1.0
0.5
0.0
Control
Piezo1 KD
E
NT
CCL19
5 µm
Paxillin
Hoechst
Merged
F
p = 0.0008
Paxillin Polarity
1.0
0.5
0.0
NT
CCL19
G
Control
Piezo1 KD
5 µm
Paxillin
Hoechst
Merged
H
ns
Paxillin Polarity
1.0
0.5
0.0
Control
Piezo1 KD
I
CCL19
CCL19 +
FAK Inhibitor 14
5 µm
Piezo1
Hoechst
Merged
J
p < 0.0001
Piezo1 Polarity Index
1.0
0.8
0.6
0.4
0.2
0.0
CCL19 + +
FAK Inhibitor 14 - +

Figure 3

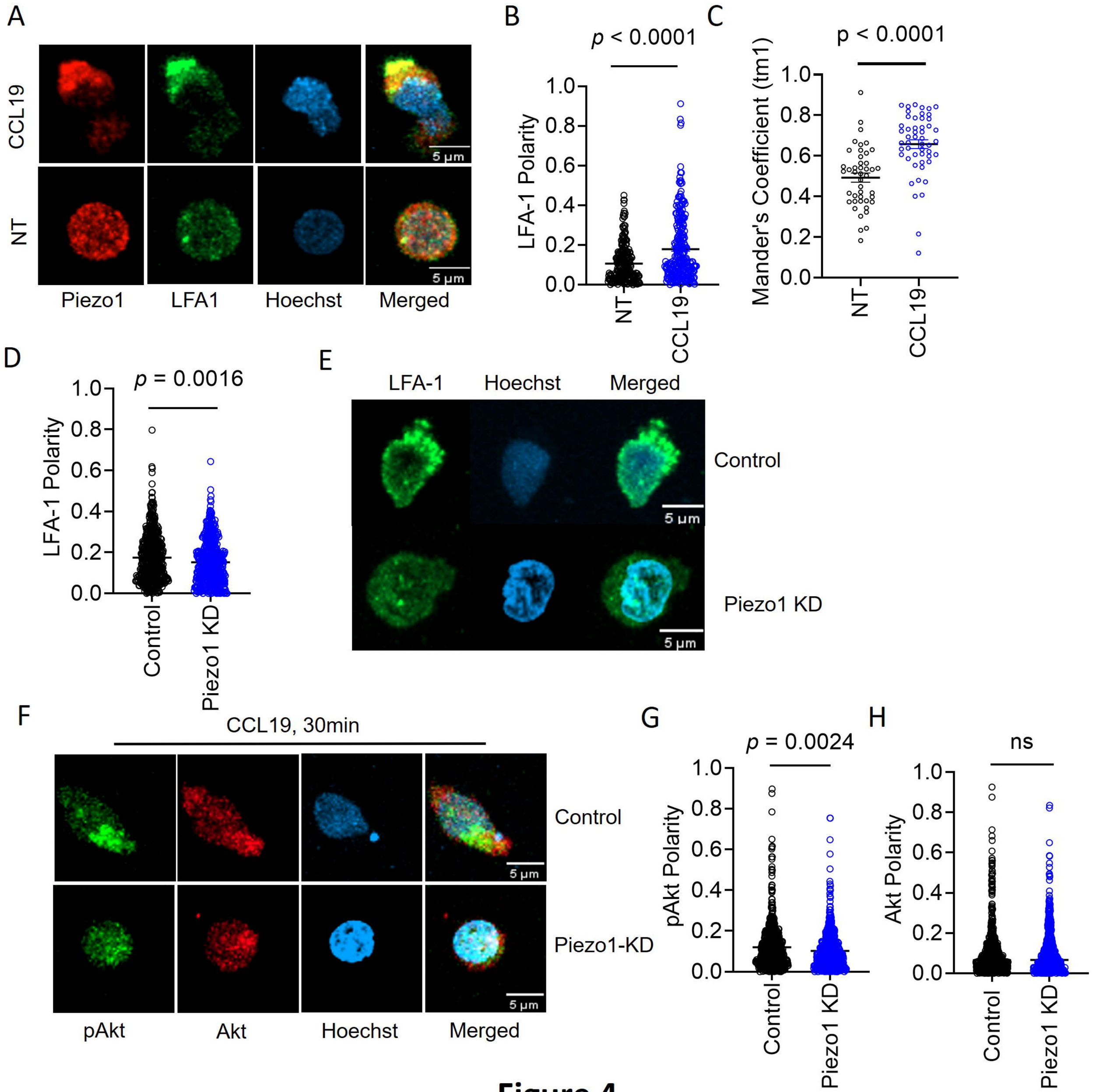
A
CCL19
NT
5 µm
5 µm
Piezo1
LFA1
Hoechst
Merged
B
p < 0.0001
LFA-1 Polarity
1.0
0.8
0.6
0.4
0.2
0.0
NT
CCL19
C
p < 0.0001
Mander's Coefficient (tm1)
1.0
0.8
0.6
0.4
0.2
0.0
NT
CCL19
D
p = 0.0016
LFA-1 Polarity
1.0
0.8
0.6
0.4
0.2
0.0
Control
Piezo1 KD
E
LFA-1
Hoechst
Merged
Control
Piezo1 KD
5 µm
5 µm
F
CCL19, 30min
Control
Piezo1-KD
5 µm
5 µm
pAkt
Akt
Hoechst
Merged
G
p = 0.0024
pAkt Polarity
1.0
0.8
0.6
0.4
0.2
0.0
Control
Piezo1 KD
H
ns
Akt Polarity
1.0
0.8
0.6
0.4
0.2
0.0
Control
Piezo1 KD

Figure 4

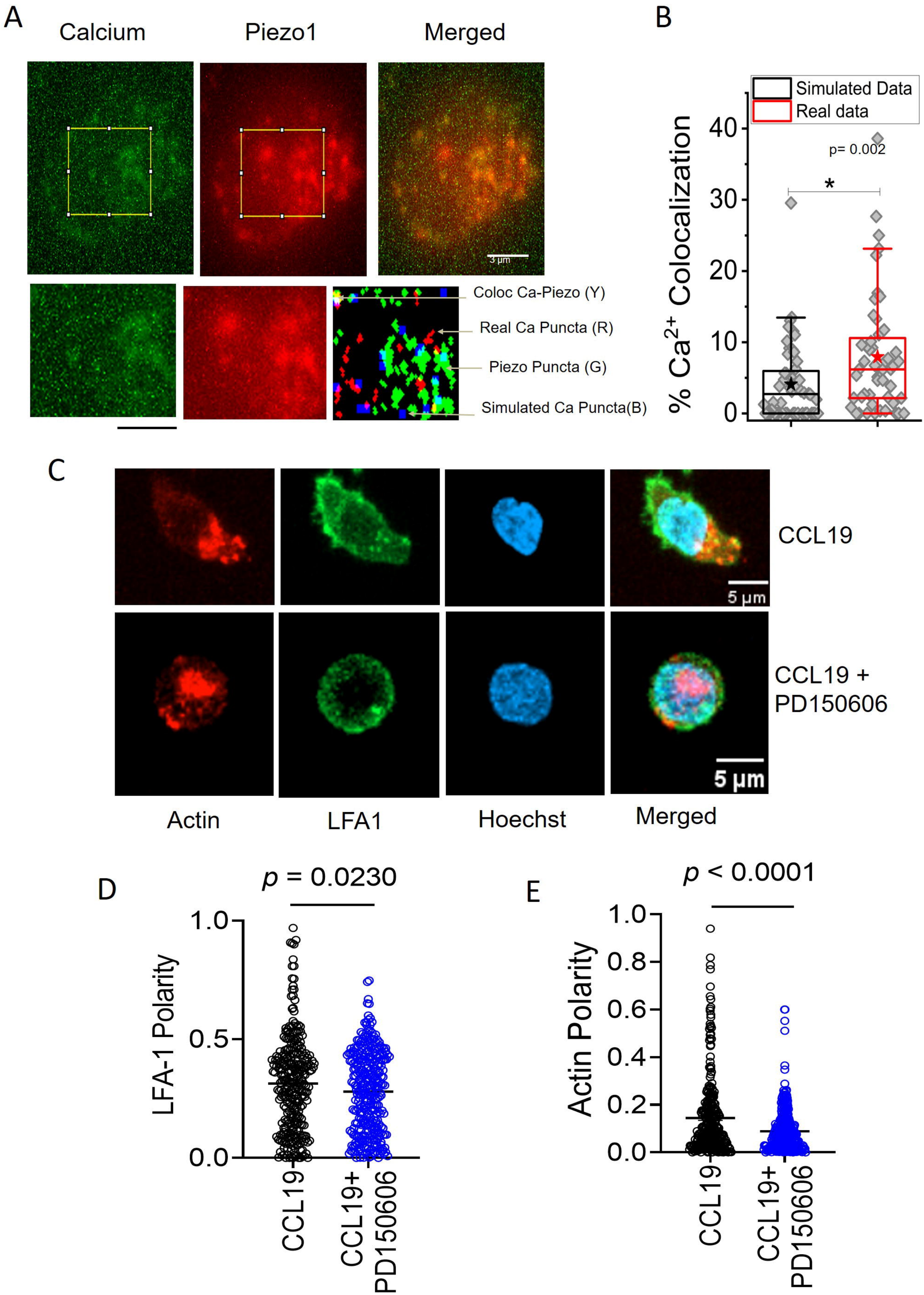
A
Calcium
Piezo1
Merged
3 µm
Coloc Ca-Piezo (Y)
Real Ca Puncta (R)
Piezo Puncta (G)
Simulated Ca Puncta(B)
B
Simulated Data
Real data
p= 0.002
*
% Ca2+ Colocalization
40
30
20
10
0
C
CCL19
5 µm
CCL19 +
PD150606
5 µm
Actin
LFA1
Hoechst
Merged
D
p = 0.0230
LFA-1 Polarity
1.0
0.5
0.0
CCL19
CCL19+
PD150606
E
p < 0.0001
Actin Polarity
1.0
0.8
0.6
0.4
0.2
0.0
CCL19
CCL19+
PD150606

Figure 5

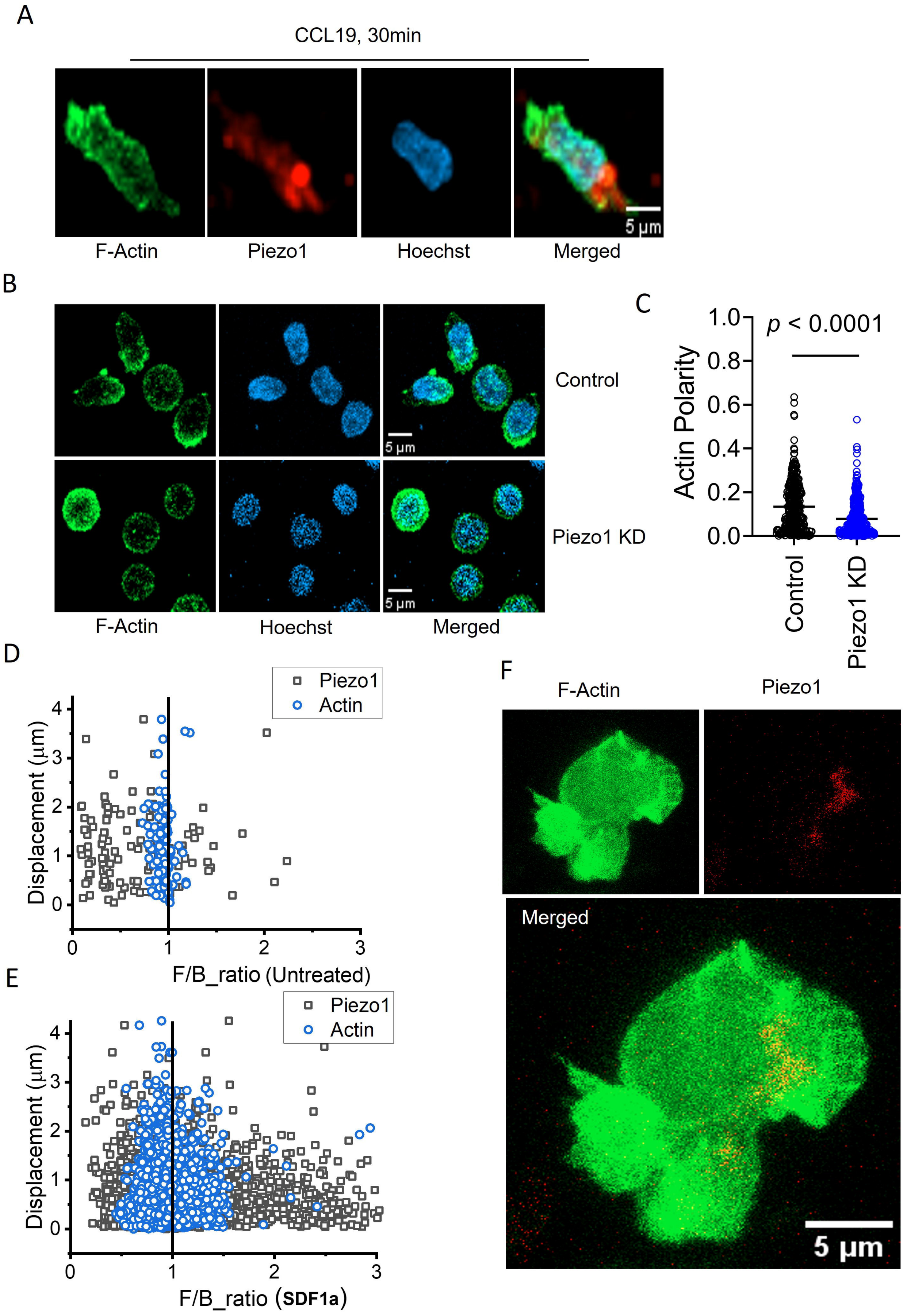
A
CCL19, 30min
F-Actin
Piezo1
Hoechst
Merged
5 µm
B
Control
Piezo1 KD
F-Actin
Hoechst
Merged
5 µm
C
p < 0.0001
Actin Polarity
1.0
0.8
0.6
0.4
0.2
0.0
Control
Piezo1 KD
D
Piezo1
Actin
Displacement (µm)
F/B_ratio (Untreated)
E
Piezo1
Actin
Displacement (µm)
F/B_ratio (SDF1a)
F
F-Actin
Piezo1
Merged
5 µm

Figure 6